

Higher Order Statistics for Three-dimensional Shear and Flexion

Dipak Munshi⁽¹⁾, Thomas Kitching⁽²⁾, Alan Heavens⁽²⁾, Peter Coles⁽¹⁾

⁽¹⁾ School of Physics and Astronomy, Cardiff University, Queen's Buildings, 5 The Parade, Cardiff, CF24 3AA, UK

⁽²⁾ Scottish Universities Physics Alliance (SUPA), Institute for Astronomy, University of Edinburgh, Blackford Hill, Edinburgh EH9 3HJ, UK

17 September 2018, Revision: 0.9

ABSTRACT

We introduce a collection of statistics appropriate for the study of spinorial quantities defined in three dimensions, focussing on applications to cosmological weak gravitational lensing studies in 3D. In particular, we concentrate on power spectra associated with three- and four-point statistics, which have the advantage of compressing a large number of typically very noisy modes into a convenient data set. It has been shown previously by Munshi & Heavens (2009) that, for non-Gaussianity studies in the microwave background, such compression can be lossless for certain purposes, so we expect the statistics we define here to capture the bulk of the cosmological information available in these higher-order statistics. We consider the effects of a sky mask and noise, and use Limber's approximation to show how, for high-frequency angular modes, confrontation of the statistics with theory can be achieved efficiently and accurately. We focus on scalar and spinorial fields including convergence, shear and flexion of 3D weak lensing, but many of the results apply for general spin fields.

Key words: : Cosmology– Weak Lensing Surveys- Large-Scale Structure of Universe – Methods: analytical, statistical, numerical

INTRODUCTION

In this paper, we consider a set of new statistics designed to encapsulate much of the information content of third-order and higher statistics for spinorial fields defined in three dimensions. In cosmological applications such higher-order statistics can be very noisy, and the dimensionality of the space may also lead to a very large number of data to consider. Thus some form of data compression is attractive, but preferably in a way which does not reduce the cosmological information content inherent in the original statistics. In this paper, we build on the ideas originally presented in Munshi & Heavens (2009), where it was shown that one statistic, the power spectrum associated with the bispectrum, could be used very effectively to estimate non-gaussianity in the microwave background radiation, as it was a lossless compression for this purpose, and also had the important added benefit of being able to provide evidence that a non-gaussianity is primordial. In this paper, we extend the ideas to cover spin-weighted fields which are defined in three dimensions, with particular emphasis on weak lensing fields convergence, shear and flexion.

Weak gravitational lensing of background source galaxies is caused by fluctuations in the intervening mass distribution. It manifests itself in a number of ways, most notably as distortions in their images. This effect arises due to the fluctuations of the gravitational potential and consequent deflection of light by gravity.

Despite being a relatively young subject weak gravitational lensing (Munshi et al. 2008) has made major progress within the last decade, since the first measurements were published (Bacon, Refregier & Ellis 2000; Wittman et al 2000; Kaiser, Wilson & Luppino 2000; Waerbeke et al 2000). There has been considerable progress in analytical modelling, technical specification and the control of systematics. By its dependence on the mass power spectrum at lower redshifts, weak lensing surveys play a complementary role to the studies based on large-scale galaxy surveys and Cosmic Microwave Background (CMB) observations. Ongoing and future weak lensing surveys such as the CFHT legacy survey¹, Pan-STARRS², the Dark Energy Survey, and further in the future, the Large Synoptic Survey Telescope³, WFIRST⁴ and Euclid⁵ will provide a wealth of information in terms of mapping the distribution of mass and energy in the universe.

Owing to the lack of photometric redshift information the traditional approach to weak lensing has largely adopted a 2D approach, analysing correlations of the shapes of galaxy images on the sky only. However the availability of photometric redshifts allows a 3D weak lensing analysis, which was introduced by Heavens (2003). Later developments by various authors (Heavens et al. 2000; Heavens et al 2006; Heavens, Kitching & Verde 2007; Castro et al 2005) have shown that it can play a vital role in constraining the dark energy equation of state (Heavens et al 2006) and the neutrino mass (Kitching et al. 2008). This

¹ <http://www.cfht.hawaii.edu/Sciences/CFHTLS/>

² <http://pan-starrs.ifa.hawaii.edu/>

³ http://www.lsst.org/lsst_home.shtml

⁴ <http://wfirst.gsfc.nasa.gov/>

⁵ <http://sci.esa.int/euclid>

arXiv:1012.3658v1 [astro-ph.CO] 16 Dec 2010

has lead to recent progress in modelling weak lensing observables in 3D extending results previously obtained in projection or using tomographic techniques (Munshi, Coles & Heavens 2010).

Early results on analytical modelling typically assumed a small survey size and adopted a 2D approach that uses a flat-sky formalism. This is related to the fact that first generation of surveys typically covered a small portion of the sky and lacked any redshift information (Jain, Seljak & White 2000). Indeed such analytical modelling was very successful in predicting lower-order statistical properties of weak lensing convergence and shear very accurately (Munshi & Jain 2001; Munshi 2000; Munshi & Jain 2000). These results depends on analytical modelling of underlying density perturbations using perturbative and empirical methods. (Munshi & Jain 2001; Valageas 2000; Munshi & Valageas 2005; Valageas, Barber, & Munshi 2004; Valageas, Munshi & Barber 2005). A tomographic step was next advocated to tighten the cosmological constraints. The tomographic studies typically divides the sources into a few redshift slices (Hu 1999; Takada & White 2003; Takada & Jain 2004; Massey et al 2007; Schrabback et al. 2009). These slices are then analyzed essentially using a two-dimensional approach but including the correlation between different redshift slices. A notable exception to the 2D analysis was Stebbins (1996) who developed an all-sky formalism for weak lensing surveys. The techniques developed in Stebbins (1996) rely on a tensorial formalism, whereas we will be using an equivalent treatment based on spin weight spherical harmonics. Extending previous studies by Heavens (2003) and Castro et al (2005), Munshi, Heavens & Coles (2010) extended the all-sky formalism to 3D to take into account the photometric redshift information, as well as extending to higher-order statistics. However they focused on the convergence field which, being a spin-0 field, is relatively easier to analyze. The main motivation behind this work is to extend previous results to arbitrary spinorial fields such as shear and their derivatives flexion.

Weak lensing at small angular scales probes the nonlinear regime of gravitational clustering, and the extra modes there can lift degeneracies about background cosmology present in studies involving the power spectrum alone see, e.g., Bernardeau, Van Waerbeke & Mellier (1997); Jain & Seljak (1997); Hui (1999); Schneider et al (2002); Takada & Jain (2003). The nonlinear regime is characterized by gravity-induced non-Gaussianity, and detailed studies that employ the Fisher matrix formalism have already demonstrated the potential of using higher-order non-Gaussianity information to lift cosmological degeneracies. Higher-order studies are also important in evaluating the variance of lower-order statistics, e.g. a proper knowledge of the trispectrum is essential for computing the error bars in the power spectrum (Takada & Jain 2009). The modelling of higher-order statistics typically involves either perturbative techniques or empirical modelling of the underlying matter clustering (Fry 1984; Schaeffer 1984; Bernardeau & Schaeffer 1992; Szapudi & Szalay 1993, 1997; Munshi et al 1999; Munshi, Coles & Melott 1999a,b; Munshi, Melott & Coles 1999; Coles, Melott & Munshi 1999; Munshi & Coles 2000, 2002, 2003). Using such prescriptions and their extensions, studies involving non-Gaussianity, have also been performed in projection (2D) as well as using tomographic information (Hu 1999; Takada & Jain 2004, 2003; Semboloni et al 2008) with remarkable success.

Studies involving higher-order correlation functions have been performed using observational data (Bernardeau, Van Waerbeke & Mellier 1997; Bernardeau, Mellier & Van Waerbeke 2002; Pen et al 2003; Jarvis, Bernstein & Jain 2004). Most of these studies involve one-point moments (cumulants) which collapse the entire correlation function into a single number. Mode-by-mode estimates of higher-order correlation functions or multispectra though far more interesting is difficult given the low signal-to-noise of current observational data. Current studies by Munshi & Heavens (2009) defined power spectra associated with each multispectrum that uses an intermediate option in data compression. While initially this concept was applied to CMB studies, recent work by (Munshi, Coles & Heavens 2010) extended this concept to weak lensing. This initial work focused on convergence κ . Being a spin-0 (scalar) object, the analysis of convergence statistics is relatively simple. In their analysis Munshi, Heavens & Coles (2010) used the similar statistics for shear and flexion fields but in projection (2D). The main motivation for the present study is to use the full 3D information (available from photometric redshift surveys) in analyzing the non-Gaussianity not only in the convergence field but also in shear and flexion. This is particularly interesting as current photometric redshift surveys with good image quality will provide a wealth of data for the analysis of weak lensing which can be used to probe cosmological information. For our study, we combine well-motivated ansatz in modelling the gravitational clustering with the Limber approximation. The results that we derive here are generic and will be useful in other areas of cosmology where integration along line of sight is involved. To keep the results simpler we will ignore the fact, that in a realistic survey, the average density of sources will decline with distance, and the distance estimated from photometry will also include error, but these are evidently important ingredients in a practical implementation of these statistics.

The expressions for higher-order multispectra generically include multidimensional integrals involving multiple spherical Bessel functions. We will be using Limber approximation to simplify these results. We will show that, at each order, we can reduce the dimensionality of these integrals to unity by using Limber approximation. This will simplify the numerical evaluations of such integrals considerably.

This paper is arranged as follows. In §2 we discuss the basic formalism of 3D weak lensing. The formalism presented here is a generalization of (Munshi, Coles & Heavens 2010) and (Munshi, Heavens & Coles 2010) and can analyze higher-order statistics of spinorial fields in 3D. In (Munshi, Coles & Heavens 2010) results were derived for higher-order statistics for the convergence and in (Munshi, Heavens & Coles 2010) the focus was on higher-order statistics of spinorial objects but in projection (2D). The notations for 3D harmonic decomposition, which will be used in the following sections are also introduced here. In §3 we introduce the models describing higher-order clustering of underlying matter which are then used to construct models for the bispectrum and trispectrum in the nonlinear regime. The results obtained are generic and can describe higher-order statistics of weak lensing convergence, shear and flexions. In §4 we focus on power spectra associated with higher-order multispectra. Results presented in this section correspond to both all-sky and patch-sky coverage. In §5 we focus on error analysis and derive results for scatter (or variance) of various estimators in the presence of observational noise and mask. Finally §6 is devoted to discussion of the results. Though we have mainly focused on weak-lensing, the general formalism developed in the paper will have wider applicability. We will use the Hierarchical ansatz to model clustering of underlying mass distribution, but the treatment can also be adopted in the context of more elaborate scenarios of clustering e.g. halo model.

2 NOTATION

This section is devoted to introducing the basic notation and formalism of 3D weak lensing. We will follow the notation used in Munshi, Coles & Heavens (2010) which is based mainly on Heavens (2003) and further developed by Castro et al (2005). The results of Castro et al (2005) were generalized by Munshi, Coles & Heavens (2010) to take into account higher-order correlations. The aim of this paper is to extend both Munshi, Coles & Heavens (2010) and Munshi, Heavens & Coles (2010) to the analysis of shear using full 3D information.

2.1 A Tale of Two Potentials

Linking the 3D lensing potential ϕ and the 3D gravitational potential Φ is crucial in connecting lensing observables to theory. In this subsection we will consider the harmonic decomposition of 3D scalar (spin-0) fields which is a step towards making this connection because examples of such fields include the scalar potentials and the convergence field κ that we encounter in weak lensing. The harmonic decomposition is most naturally done using eigenfunctions that can be constructed using ordinary spherical harmonics and spherical Bessel functions. In the next subsection we will generalize them to the case of spinorial fields.

The statistics of shear and convergence can be expressed in a natural way through their relation to $\Phi(r, \theta, \varphi)$ the 3D gravitational potential at a 3D position r, θ, φ , and $\phi(\mathbf{r})$ the lensing potential. The density contrast $\delta(\mathbf{r})$ is directly related to the potential through the Poisson equation. This allows us to link directly the statistics of the weak lensing observables to the underlying statistics of the mass distribution, and hence to cosmological parameters. The radial distance $r(t)$ is related to the Hubble expansion parameter $H(t) = \dot{a}/a$ by $r(z) = c \int_0^z dz'/H(z')$. The Hubble parameter is sensitive to the contents of the Universe thereby making weak lensing a useful probe to study dark energy. The line of sight integral relating the two potentials can be written as (Kaiser 1992):

$$\phi(\mathbf{r}) \equiv \phi(r, \hat{\Omega}) = \frac{2}{c^2} \int_0^r dr' F_K(r, r') \Phi(r', \hat{\Omega}); \quad F_K(r, r') \equiv \frac{f_K(r - r')}{[f_K(r) f_K(r')]} \quad (1)$$

The Born approximation was used to derive the above expression (Bernardeau, Van Waerbeke & Mellier 1997; Schneider et al 2002; Waerbeke et al 2002). The lensing potential $\phi(\mathbf{r}) \equiv \phi(r, \hat{\Omega})$ has a radial dependence and is a 3D quantity. In our notation $r = r(t)$ is the comoving distance to the source whose observed light was emitted at a given instance of time t . The observer is situated at the origin. The function $F_K(r, r')$ depends on the background cosmology. through the function $f_K(r)$; $f_K(r) = \sin r, r, \sinh r$ for a closed ($K = 1$), flat ($K = 0$) or open ($K = -1$) universes respectively. Our convention for the Fourier transform for the 3D fields is as in Munshi, Coles & Heavens (2010). The eigenfunctions of the Laplacian operator in flat space when expressed in spherical coordinates turn out to be a product of spherical Bessel functions $j_l(kr)$ in the radial direction and the spherical harmonics on the surface of a unit sphere i.e. $Y_{lm}(\hat{\Omega}) = Y_{lm}(\theta, \phi)$. The eigenfunctions $Z_{klm}(\mathbf{r}) = \sqrt{\frac{2}{\pi}} k j_l(kr) Y_{lm}(\hat{\Omega})$ are associated with eigenvalues $-k^2$. In general the radial eigenfunctions are ultra-spherical Bessel functions, but they can be approximated by spherical Bessel functions when the curvature is small. The eigendecomposition and its inverse transformation can be expressed as:

$$\Phi_{lm}(k) = \int d^3\mathbf{r} \Phi(\mathbf{r}) Z_{klm}(\mathbf{r}); \quad (2)$$

and

$$\Phi(\mathbf{r}) = \sum_{l=0}^{\infty} \sum_{m=-l}^{m=l} \int dk \Phi_{lm}(k) Z_{klm}(\mathbf{r}). \quad (3)$$

The specific choice of eigenfunctions allows us easily to express the coefficients of expansion of the convergence (or shear) in terms of the expansion of the density field through the Poisson equation (Heavens 2003) $\Delta\Phi(\mathbf{r}) = 3\Omega_m H_0^2 \delta(\mathbf{r})/2a$. In the harmonic domain this can be expressed as $\Phi_{lm}(k; r) = A \delta_{lm}(k; r)/a(r) k^2$ with $A \equiv -3\Omega_m H_0^2/2$. Here, $\Phi_{lm}(k)$ is the spherical harmonic decomposition of $\Phi(\mathbf{r})$, and similarly for $\phi(\mathbf{r})$. In our notations, $a(z) = 1/(1+z)$ is the scale factor at redshift z , Ω_m is the total matter density at $z = 0$, and H_0 is the Hubble constant today. $\delta_{lm}(k; r)$ is the eigendecomposition of $\delta(\mathbf{r})$. When appearing after the semi-colon, the r dependence (e.g. of $\Phi_{lm}(k; r)$) is really an expression of the time-dependence of the potentials, which translates to a dependence on r , as r depends on look-back time. Using these decompositions, the harmonic decomposition of the lensing potential $\phi_{lm}(k)$ and the 3D gravitational potential $\Phi_{lm}(k, r)$ are related by the following expression (Castro et al 2005):

$$\phi_{lm}(k) = \frac{4k}{\pi c^2} \int_0^\infty dk' k' \int_0^\infty r^2 dr j_l(kr) \int_0^r dr' F_K(r, r') j_l(k'r') \Phi_{lm}(k'; r'). \quad (4)$$

The basis functions for the harmonic decomposition of the spinorial fields such as flexion and shear will involve spin-weight spherical harmonics which we will introduce next. The 3D power spectra for the gravitational potentials Φ and the lensing potential ϕ are defined through the following expressions:

$$\langle \Phi_{lm}(k) \Phi_{l'm'}(k') \rangle = \mathcal{C}_l^{\Phi\Phi}(k) \delta_{1D}(k+k') \delta_{ll'}^K \delta_{mm'}^K; \quad \langle \phi_{lm}(k) \phi_{l'm'}(k') \rangle = \mathcal{C}_l^{\phi\phi}(k, k') \delta_{ll'}^K \delta_{mm'}^K. \quad (5)$$

2.2 3D Eigendecomposition of Spinorial Functions

In this subsection we will introduce the generic spin-weight functions and their eigendecomposition. Specific cases that are of interest here include shear and flexions. This will generalize the spin-0 results discussed above for the convergence field. We can expand the fields such as shear $\gamma_{\pm}(\mathbf{r})$, flexions $\mathcal{F}(\mathbf{r}), \mathcal{G}(\mathbf{r})$ in 3D basis functions that are constructed out of spin-weight spherical harmonics ${}_s Y_{lm}(\hat{\Omega})$ on the celestial sphere and spherical Bessel functions $j_l(kr)$ in the radial direction. Expansion in such bases provides a very simple relationship between harmonic coefficients of the shear, flexion and convergence on the one hand, and the lensing potentials on the other. Moreover, spherical coordinates are the natural choice for eigendecomposition as this provides a clear separation in terms of radial modes and the modes on the surface of the sky, and the ubiquitous presence of a sky mask induces mixing of modes only on the surface of the sphere, and the use of photometric redshift estimates only introduces error in the radial direction without altering the angular position. The choice of eigenfunction is also motivated by the Poisson equation which relates the 3D potential $\Phi(\mathbf{r})$ to the density distribution $\delta(\mathbf{r})$, whose statistical property we will model to predict the statistics of shear, convergence or flexion. Extending the definition of spin-0 eigenfunctions $Z_{klm}(\mathbf{r})$ we will denote the spin- s eigenfunctions as ${}_s Z_{klm}(\mathbf{r})$; which is defined as: ${}_s Z_{klm}(\mathbf{r}) = \sqrt{\frac{2}{\pi}} k j_l(kr) {}_s Y_{lm}(\hat{\Omega})$. The spin-weight spherical harmonics are defined in terms of D-matrices (Varshalovich, Moskalev & Khersonskii 1988; Penrose & Rindler 1984, 1986). They satisfy a orthogonality relationship similar to ordinary

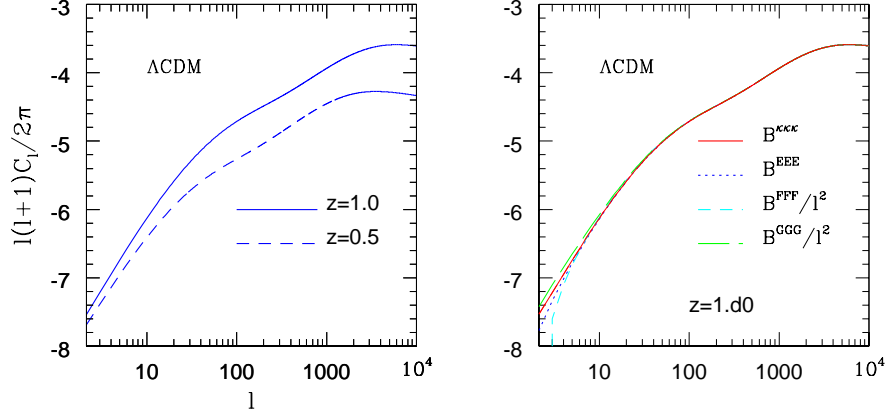


Figure 1. Left panel compares the power spectrum C_l for the convergence κ for two different source redshift $z_s = 1$ and $z_s = 0.5$. Right panel shows the power spectrum C_l for the convergence κ , electric part of the shear E , flexions \mathcal{F} and \mathcal{G} as a function of l . The flexion power spectra $C_l^{\mathcal{F}}, C_l^{\mathcal{G}}$ are normalized by l^2 for display. The cosmology assumed is Λ CDM and all sources are assumed to be at the same redshift of $z_s = 1$. The Λ CDM background cosmology that we have considered is described by the following set of parameters: $\Omega_m = 0.3, \Omega_\Lambda = 0.7, \Gamma = 0.21, h = 0.7$ and $\sigma_8 = 0.90$.

spherical harmonics. Spin-weight harmonics with the same or different spin indices are orthogonal on the surface of sky. This generalizes the orthogonality relationship of ordinary spin-zero spherical harmonics: ${}_s Y_{lm}(\hat{\Omega}) = \sqrt{\frac{2l+1}{4\pi}} D_{-s,m}^l(\theta, \phi, 0), \int d\hat{\Omega} {}_s Y_{lm}(\hat{\Omega}) {}_{s'} Y_{l'm'}^*(\hat{\Omega}) d\hat{\Omega} = \delta_{ll'} \delta_{mm'} \delta_{ss'}$.

Alternative expansion schemes are indeed possible such as using tensor spherical harmonics but they are perhaps more difficult to work with. It is worth noting here that the formalism of spin-harmonics is extensively used in studies involving Cosmic Microwave Background Polarization (Bunn et al 2003). The forward and inverse transform of an arbitrary spin function ${}_s f(\mathbf{r})$ from real space to harmonic space links it with its harmonic components ${}_s f_{lm}(k)$ that can be expressed as: ${}_s f(\mathbf{r}) = \int_0^\infty dk \sum_{l=0}^\infty \sum_{m=-l}^{m=l} [{}_s f_{lm}(k)] {}_s Z_{klm}(\mathbf{r})$ and ${}_s f_{lm}(k) = \int d^3\mathbf{r} [{}_s f(\mathbf{r})] {}_s Z_{klm}^*(\mathbf{r})$. The orthogonality relationship satisfied by the 3D spherical basis functions $[{}_s Z_{klm}(\mathbf{r})]$ depends on the orthogonality of spin-weight harmonics ${}_s Y_{lm}(\hat{\Omega})$ and that of the spherical Bessel functions $j_l(kr)$. It generalizes a similar relation for the scalar harmonics. For arbitrary spinorial fields with spins s and s' it reads: $\int d^3\mathbf{r} [{}_s Z_{klm}(\mathbf{r})] [{}_{s'} Z_{k'l'm'}^*(\mathbf{r})] = \delta_D(k - k') \delta_{ll'} \delta_{mm'} \delta_{ss'}$. The inverse transforms are used to define the harmonic components of generic spinorial fields $\eta(\mathbf{r})$ and $\eta^*(\mathbf{r})$. The results that we will derive in our later sections are expressed most naturally in the harmonic domain using these components ${}_2\eta_{lm}(k)$ and ${}_{-2}\eta_{lm}(k)$ which can be expressed as: ${}_2\eta_{lm}(k) = \int d^3\mathbf{r} \eta(\mathbf{r}) {}_2 Z_{klm}(\mathbf{r})$ and ${}_{-2}\eta_{lm}(k) = \int d^3\mathbf{r} \eta^*(\mathbf{r}) {}_{-2} Z_{klm}(\mathbf{r})$. It is indeed possible to work with ${}_2\eta_{lm}(k)$ and ${}_{-2}\eta_{lm}(k)$ as well as the harmonics $E_{lm}(k)$ and $B_{lm}(k)$ that can be constructed from them. Though they contain the same information, the *Electric* or *E* and *Magnetic B* modes provides a rotationally invariant description in full sky. The expansion coefficients E_{lm} has a parity $(-1)^l$ while B_{lm} has a parity $(-1)^{l+1}$. The clear separation of modes with different parity gives a clear mathematical advantage in the case of weak lensing, as It can be shown that, at first order, weak lensing from gravitational clustering can only generate *E* modes, whereas systematics are mostly responsible for the generation of any *B* mode contribution.

The explicit expressions for the electric $E_{lm}(k)$ and magnetic $B_{lm}(k)$ components, constructed from these harmonic transforms are: $E_{lm}(k) = -\frac{1}{2}[{}_2\eta_{lm}(k) + {}_{-2}\eta_{lm}(k)]$; $B_{lm}(k) = \frac{i}{2}[{}_2\eta_{lm}(k) - {}_{-2}\eta_{lm}(k)]$; and ${}_{\pm 2}\eta_{lm}(k) = -[E_{lm}(k) \pm iB_{lm}(k)]$. The individual components of the field $\eta(\mathbf{r})$, $\eta_1(\mathbf{r})$ and $\eta_2(\mathbf{r})$ are expressed in terms of eigenfunctions $Z_{+,klm}(\mathbf{r})$ that can be constructed from linear combinations of $Z_{\pm 2,klm}(\mathbf{r})$ introduced before. The formalism used here is very similar to Munshi, Heavens & Coles (2010). The emphasis here however is not just on 2D decomposition on the surface of the celestial sphere but rather on a 3D decomposition which relies on the photometric redshift to estimate radial distance.

It is worth mentioning here that unique decomposition of a function into modes *E* and *B* mode on the celestial sphere is possible only with complete sky coverage. In the presence of a boundary, which is often the case owing to the presence of masks, the decomposition is ambiguous. For the case of weak lensing shear these equations can be specialized further by ignoring the magnetic contribution which is zero for shear generated purely by gravitational lensing in the absence of any systematics. Indeed, higher-order lensing corrections can generate lensing *B* mode too (Cooray & Hu 2002) but are sub-dominant.

2.3 Harmonic decomposition of Convergence, Shear and Flexion

The results derived in previous section can directly be applied to the case of flexions, shear and convergence. Most of the generic results are applicable to the analysis of shear γ if we specialize the field η with a spin-2 object and identify with 3D shear γ . Complex shear γ constructed from its individual components $\gamma_{\pm}(\mathbf{r}) = \gamma_1(\mathbf{r}) \pm i\gamma_2(\mathbf{r})$ acts as a spin-2 object and can be expressed in terms of the lensing potential ϕ using spin-derivatives (see Munshi, Heavens & Coles (2010) and Castro et al (2005) for more discussion on spin-derivatives) which are used to construct spinorial fields with different spin-weights. The lensing potential plays the role of the generic scalar field introduced earlier to express arbitrary spin functions. We will use the same symbol ϕ for both. We will use the generalized symbol ${}_s\Gamma$ for general spin fields which will include products of shear fields as well as higher derivative spin objects such as flexions. In our current notation ${}_2\Gamma = \gamma$ and ${}_{-2}\Gamma = \gamma^*$: ${}_2\Gamma(\mathbf{r}) \equiv \gamma(\mathbf{r}) = \frac{1}{2}\bar{\partial}\bar{\partial}[\phi]$ and ${}_{-2}\Gamma(\mathbf{r}) \equiv \gamma^*(\mathbf{r}) = \frac{1}{2}\bar{\partial}\bar{\partial}[\phi^*]$. In general the scalar potential $\phi(\mathbf{r})$ will have both electric $\phi_E(\mathbf{r})$ and magnetic $\phi_B(\mathbf{r})$ components: $\phi(\mathbf{r}) = \phi_E(\mathbf{r}) + i\phi_B(\mathbf{r})$.

The individual shear components $\gamma_1(\mathbf{r})$ and $\gamma_2(\mathbf{r})$ and the convergence $\kappa(\mathbf{r})$ can be expressed in terms of a complex lensing potential $\phi(\mathbf{r}) = \phi_E(\mathbf{r}) + i\phi_B(\mathbf{r})$. As pointed out before the magnetic part of the potential $\phi_B(\mathbf{r})$ will take contribution mainly from systematics and the electric part corresponds largely to pure lensing contribution $\gamma_1(\mathbf{r}) = \frac{1}{4}(\bar{\partial}\bar{\partial} + \bar{\partial}\bar{\partial})\phi(\mathbf{r})$; $\gamma_2(\mathbf{r}) = -\frac{i}{4}(\bar{\partial}\bar{\partial} - \bar{\partial}\bar{\partial})\phi(\mathbf{r})$ and $\kappa(\mathbf{r}) = \frac{1}{4}(\bar{\partial}\bar{\partial} + \bar{\partial}\bar{\partial})\phi(\mathbf{r})$.

Derivatives of the shears are higher-spin objects. Using these derivatives quantities such as *flexions* are constructed, which are also often used in the

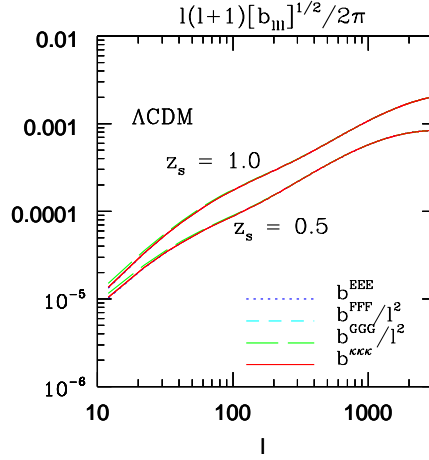


Figure 2. The diagonal components of the reduced convergence bispectrum b_{III} are plotted as function of l . The bispectrum is assumed to have a hierarchical form. The hierarchical amplitude Q_3 is set to unity. The source redshift is set to unity $z_s = 1$. The plots for the flexions \mathcal{F} and \mathcal{G} are normalized by l^2 for display.

context of weak lensing studies (Goldberg & Natarajan (2002); Goldberg & Bacon (2005); Bacon et al. (2006); Bacon & Goldberg (2005); Schneider & Er (2008)). The two flexions that are most commonly used are also known as the first flexion \mathcal{F} (spin -1) and \mathcal{G} which is also known as the second flexion (spin 3). These two flexions in combination can specify distortion beyond what is described by shear. The flexions can be used to describe weak “arciness” in images of lensed galaxies and their relationship with the shapelet formalism is well documented (Refregier 2003; Bernstein & Jarvis 2002; Refregier & Bacon 2003). The flexions $\mathcal{F}(\mathbf{r})$ and $\mathcal{G}(\mathbf{r})$ are both used in the literature mainly for individual halo profiles and also for the study of substructures (Bacon et al. 2006). We are mainly interested however in higher-order statistics of these objects for generic underlying cosmological clustering. This is done by linking the 3D harmonic decompositions of the flexions to that of the lensing potential $\phi(\mathbf{r})$: $\mathcal{F}(\mathbf{r}) = \frac{1}{6}(\bar{\partial}\bar{\partial}\bar{\partial} + \bar{\partial}\bar{\partial}\bar{\partial})\phi(\mathbf{r})$ and $\mathcal{G}(\mathbf{r}) = \frac{1}{2}\bar{\partial}\bar{\partial}\bar{\partial}\phi(\mathbf{r})$. Flexions have been used primarily to measure the galaxy-galaxy lensing to probe the galaxy halo density profiles. Their cosmological use will depend on an accurate understanding of gravitational clustering at small angular scales.

In Fourier space the harmonics of $\gamma(\mathbf{r})$ and $\gamma^*(\mathbf{r})$ can be expressed in terms of the harmonic coefficients of $\Phi_E(\mathbf{r})$ and $\Phi_B(\mathbf{r})$ denoted by $E_{lm}(k)$ and $B_{lm}(k)$ respectively: $\pm_2\Gamma_{lm}(k) = -[E_{lm}(k) \pm iB_{lm}(k)]$. Analogously, the harmonics of \mathcal{F} and \mathcal{G} denoted by $\mathcal{F}_{lm}(k)$ and $\mathcal{G}_{lm}(k)$ can also be expressed in terms of the $\phi_{lm}(k)$. In the absence of B-modes the harmonics of the shear components are directly related to the harmonic component of the Electric field E_{lm} . The harmonic transforms of the shear components and convergence can also be expressed in terms of the lensing potential ϕ as follows: $\kappa_{lm}(k) = -\frac{l(l+1)}{2}\phi_{lm}(k)$; $E_{lm}(k) = -\frac{1}{2}\sqrt{\frac{(l+2)!}{(l-2)!}}\phi_{lm}(k)$; $\mathcal{F}_{lm}(k) = \frac{1}{6}l^{1/2}(l+1)^{1/2}(3l^2 + 3l - 2)\phi_{lm}(k)$; $\mathcal{G}_{lm}(k) = \frac{1}{2}\sqrt{\frac{(l+3)!}{(l-3)!}}\phi_{lm}(k)$.

These harmonic expressions can be used to reconstitute the real space spinorial fields: $\pm_2\Gamma(\mathbf{r}) = \int kdk \sum_{l=0}^{\infty} \sum_{m=-l}^l \sqrt{\frac{(l+2)!}{(l-2)!}} \phi_{lm}(k) \pm_2 Z_{klm}(\mathbf{r}, \hat{\Omega})$; $\mathcal{F}(\mathbf{r}) = \int kdk \sum_{l=0}^{\infty} \sum_{m=-l}^l \mathcal{F}_{lm}(k) {}_{-1}Z_{klm}(\mathbf{r})$ and $\mathcal{G}(\mathbf{r}) = \int kdk \sum_{l=0}^{\infty} \sum_{m=-l}^l \mathcal{G}_{lm}(k) {}_3Z_{klm}(\mathbf{r})$. These results derived above are useful in linking the statistics of weak lensing fields $\kappa(\mathbf{r})$, $\gamma(\mathbf{r})$, $\mathcal{F}(\mathbf{r})$ and $\mathcal{G}(\mathbf{r})$ with those of the underlying density field $\delta(\mathbf{r})$ responsible for generation of the lensing potential $\phi(\mathbf{r})$ with the help of Eq.(4).

The theoretical modelling of the underlying mass distribution that we employ in our study is based on the hierarchical ansatz. The hierarchical ansatz is more suited to model gravitational clustering a smaller scales, which makes it particularly suitable for modelling the flexion statistics which put more weight on smaller scales. A comment about noise contribution due to intrinsic flexions of source galaxies is in order. While it is relatively easy to model the intrinsic ellipticity of source galaxies, detailed modelling of intrinsic flexion of source galaxies is much more complicated and depends heavily on modelling of galaxy shapes beyond the simplest description. This uncertainty is also expected to increase with survey depth.

In addition to shear, convergence and flexion which are used in weak lensing studies, we can also consider a generic scalar tracer field Ψ in our study. Such fields can represent a suitable large scale tracers which are sometimes used for cross-correlation studies or studies involving weak lensing magnification.

The statistics of shear and flexions can be best related to that of convergence with certain l dependent multiplicative factors that we will call *form factors*. In later sections F_l^Γ will denote the form factor associated with a generic spin-weight field Γ . So the form factor for the shear γ_{\pm} will be denoted by $F_l^{\gamma_{\pm}}$.

3 3D WEAK LENSING STATISTICS: POWER SPECTRUM AND BEYOND

For the study of non-Gaussianity we need to go beyond the study of power spectra. In this section we will present results for 2-, 3- and 4-point statistics, and show the relation between observables and theory. The various multispectra involve multidimensional integrals, which we simplify by employing various levels of approximations involving the high l behaviour of $j_l(x)$.

3.1 Power spectrum

We will start by deriving the power spectrum $C_l^{\Gamma\Gamma'}(k_1, k_2)$ for the 3D weak lensing fields. Our derivation of the 3D convergence power spectrum is based on expressing its harmonic coefficients $\kappa_{lm}(k)$ in terms of the 3D density field δ with the help of Poisson’s equation and using the definition of the convergence field in terms of the projected lensing potential ϕ gives:

$$\kappa_{lm}(k) = \frac{2kA}{\pi c^2} l(l+1) \int_0^\infty dk' k' \int_0^\infty r^2 dr j_l(kr) \int_0^r dr' F_K(r, r') j_l(k' r') \frac{\delta_{lm}(k'; r')}{k'^2 a(r')} \quad (6)$$

We will use a shorthand notation $I_l(k_i, k)$ (defined below) useful for simplification of our results. We will approximate the cross-spectra at two different epoch using the approximation $P^{\Phi\Phi}(k, r, r') = \sqrt{P^{\Phi\Phi}(k, r)P^{\Phi\Phi}(k, r')}$ (Castro et al 2005). Use of this approximation leads to separation of respective integrals. As we will see below the use of the extended Limber approximation, which is valid at high l , implies that dominant contribution will come from single time slices $r = r'$ and this approximation is not detrimental to any of the final results which are quite generic. The 3D power spectrum can be expressed in terms of $I_l(k_i, k)$ as Castro et al (2005):

$$I_l(k_i, k) \equiv k_i \int_0^\infty dr r^2 j_l(k_i r) \int_0^r dr' F_K(r, r') j_l(kr') \sqrt{P^{\Phi\Phi}(k; r')} \\ \mathcal{C}_l^{\phi\phi}(k_1, k_2) = \frac{16}{\pi^2 c^4} \int_0^\infty k^2 I_l(k_1, k) I_l(k_2, k) dk; \quad \mathcal{C}_l^{\kappa\kappa}(k_1, k_2) = \frac{1}{4} l^2 (l+1)^2 \mathcal{C}_l^{\phi\phi}(k_1, k_2); \quad \mathcal{C}_l^{\Gamma\Gamma'}(k_1, k_2) = F_l^\Gamma F_l^{\Gamma'} \mathcal{C}_l^{\kappa\kappa}(k_1, k_2). \quad (7)$$

Clearly the above expression is quite generic and contains all the weak lensing information at the second-order level. This expression is however quite cumbersome for any numerical implementation as it involves three-dimensional integral which are quite demanding computationally. We will be using extended Limber approximation valid at high l to simplify the above expression. Using this approximation we can reduce the integrals to one-dimensional integrals. In any case we will quote the generic result that is valid without any approximation. Notice that the following approximation is also independent of the factorization of the power spectrum introduced before.

$$\mathcal{C}_l^{\phi\phi}(k_1, k_2) = \frac{16}{\pi^2 c^4} \int k^2 dk I_l(k_1, k) I_l(k_2, k) \\ = \frac{16}{\pi^2 c^4} k_1 k_2 \int_0^\infty dr_a r_a^2 j_l(k_1 r_a) \int_0^r dr'_a F_K(r_a, r'_a) \int_0^\infty dr_b r_b^2 j_l(k_1 r_b) \int_0^r dr'_b F_K(r_b, r'_b) \int k^2 dk P^{\Phi\Phi}(k, r'_a, r'_b) j_l(kr'_a) j_l(kr'_b). \quad (8)$$

We will next use the Limber approximation Eq.(A2) to simplify the k integral which produces a $\delta_{1D}(r'_a - r'_b)$ function. Integrating out r'_b with the help of the delta function and renaming the dummy variable r'_a to r' we can finally write:

$$\mathcal{C}_l^{\kappa\kappa}(k_1, k_2) = \frac{2}{\pi} k_1 k_2 \int_0^\infty r_1^2 dr_1 j_l(k_1 r_1) \int_0^\infty r_2^2 dr_2 j_l(k_2 r_2) \mathcal{D}_l^{\kappa\kappa}(r_1, r_2); \\ \mathcal{D}_l^{\kappa\kappa}(r_1, r_2) = \frac{A^2}{c^4} \int_0^{r_{min}} r'^2 \frac{dr'}{a^2(r')} F_K(r_1, r') F_K(r_2, r') P_\delta\left(\frac{l}{r'}; r'\right); \quad r_{min} = \min(r_1, r_2). \quad (9)$$

Use of the Limber approximation projects multi-time correlators to a single time correlator. Going one step further, If we use the high l approximation to the spherical Bessel function Eq.(A3) to reduce the dimensionality of the above integrals involving the spherical Bessel functions j_l , we arrive at the following simpler approximate equation. Use of Eq.(A3) allows us to replace r_1 and r_2 in terms of k_1, k_2 and l .

$$\mathcal{C}_l^{\kappa\kappa}(k_1, k_2) = [Ac^{-2}]^2 \left[\frac{2}{2l+1} \right] \left[\frac{2l+1}{2k_1} \right]^2 \left[\frac{2l+1}{2k_2} \right]^2 \int_0^{r_{min}} r'^2 \frac{dr'}{a^2(r')} F_K \left[\frac{2l+1}{2k_1}, r' \right] F_K \left[\frac{2l+1}{2k_2}, r' \right] P_\delta \left(\frac{l}{r'}; r' \right). \quad (10)$$

We can define a statistic $\Sigma(k_1, k_2)$ which will include all available information from individual harmonics. as a function of k_1, k_2 :

$$\Sigma^{\kappa\kappa}(k_1, k_2) = \sum_l (2l+1) \mathcal{C}_l^{\kappa\kappa}(k_1, k_2); \quad \Sigma^{\kappa\kappa}(r_1, r_2) = \sum_l (2l+1) \mathcal{C}_l^{\kappa\kappa}(r_1, r_2). \quad (11)$$

We have ignored angular smoothing in our derivation. Typically observations will involve a smoothing filter. Tophat and compensated filters are the ones that are most commonly used that can be incorporated in . As pointed out before the above equation is derived using very general arguments. It is valid at high l as the derivation is based only on high l approximation to the spherical Bessel function $j_l(x)$. Nevertheless the derivation of a 3D skew spectrum has wider applicability in cosmology. The technique can be applied to compute 3D power spectrum in other context (e.g. integrated Sachs-Wolfe effect or Kinetic Sunyaev-Zeldovich effect). Detailed analysis for such cases will be presented elsewhere.

We have used Limber approximation to simplify results LoVerde & Afshordi (2008). It was pointed out by LoVerde & Afshordi (2008) that using l instead of $l + \frac{1}{2}$, as is often done in the literature, spoils the accuracy of Limber approximation to $\mathcal{O}(\frac{1}{l})$. In general the error in Limber approximation will scale as $\mathcal{O}(\frac{1}{l^4})$. A series expansion of spherical Bessel function can also be performed to construct the next to leading order terms which further improve the accuracy of Limber approximation.

Weak lensing not only induces correlations among ellipticities of background galaxies (shear), it also introduces local modification in the number density of source galaxies (also know as weak lensing magnification). The weak lensing magnification μ is directly linked to the convergence κ . While we have focused on shear γ_\pm in this paper we plan to extend the results to magnification in a related publication.

While the results derived above are valid for all-sky surveys, observations invariably will introduce mask. We will next analyze the case of 3D power spectrum estimation in the presence of a general mask. The results that we derive will have general applicability and will be valid for near all-sky coverage.

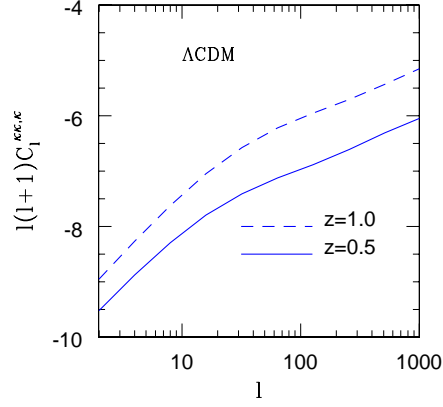


Figure 3. The skew spectrum $C_l^{\kappa,\kappa,\kappa}$ defined in Eq.(3.1) for the convergence κ is plotted as a function of l for two different source redshifts $z_s = 1$ (upper curve) and $z_s = 0.5$ (lower curve). A hierarchical form for the bispectrum was assumed and the hierarchical amplitude is set to unity. As Λ CDM background cosmology is assumed. We have not incorporated any smoothing window - calculations are done by introducing a sharp cutoff at $l_{max} = 2000$.

3.1.1 The Effect of an angular sky Mask

We start by 3D decomposition of an arbitrary spinorial field ${}_s\Gamma$ in the presence of a sky mask $w(\hat{\Omega})$, which is equal to 0 or 1 in simple cases. The decomposition into radial harmonics, using spherical Bessel functions $j_l(kr)$, can be performed independent of the mask. The harmonic decomposition on the surface of the celestial sphere involves spin-weight spherical harmonics ${}_sY_{lm}(\hat{\Omega})$. The following expression relates the masked observed harmonics $[{}_s\Gamma w]_{lm}(k)$ and he unmasked ${}_s\Gamma_{lm}(k)$. We will leave the spinorial field ${}_s\Gamma$ arbitrary and derive the expression of the cross-correlation power spectrum, in the presence of a mask, with another arbitrary spinorial field ${}_{s'}\Gamma'(\hat{\Omega})$. The results are generic and do not depend on any specific assumption that is used to model the all-sky power spectrum itself.

$$\begin{aligned} [{}_s\tilde{\Gamma}]_{lm}(k) &\equiv [{}_s\Gamma w]_{lm}(k) \equiv \sqrt{\frac{2}{\pi}} \int d^3\mathbf{r} k j_l(kr) [{}_sY_{lm}^*(\hat{\Omega})] [{}_s\Gamma(\mathbf{r})w(\hat{\Omega})] = \sqrt{\frac{2}{\pi}} \int kr^2 dk j_l(kr) \int d\hat{\Omega} [{}_s\Gamma(\mathbf{r})w(\hat{\Omega})] [{}_sY_{lm}^*(\hat{\Omega})] \\ &= \sum_{l_b m_b} \left[\sqrt{\frac{2}{\pi}} \int dk k r^2 j_l(kr) {}_s\Gamma_{l'm'}(r) \right] w_{l_a m_a} \int [{}_sY_{l'm'}(\hat{\Omega})] [Y_{l_a m_a}(\hat{\Omega})] [{}_sY_{lm}^*(\hat{\Omega})] d\hat{\Omega} \\ &= \frac{2}{\pi} \sum_{l'm'} \sum_{l_b m_b} (-1)^{s+m} \int dr \int dk' k' r^2 j_l(kr) j_{l'}(k'r) {}_s\Gamma_{l_2 m_2}(k') w_{l_a m_a} J_{l'l_a l} \begin{pmatrix} l' & l_a & l \\ s & 0 & -s \end{pmatrix} \begin{pmatrix} l' & l_a & l \\ m' & m_a & -m \end{pmatrix}; \end{aligned} \quad (12)$$

$$\approx \sum_{l'm'} \sum_{l_a m_a} (-1)^{s+m} \frac{(2l'+1)^{\frac{1}{2}}}{(2l+1)^{\frac{1}{2}}} {}_s\Gamma_{lm} \left[\frac{2l+1}{2l'+1} k \right] w_{l_a m_a} J_{l'l_a l} \begin{pmatrix} l' & l_a & l \\ s & 0 & -s \end{pmatrix} \begin{pmatrix} l' & l_a & l \\ m' & m_a & -m \end{pmatrix}. \quad (13)$$

The masked cross-spectrum $C_l^{\Gamma\Gamma'}(k, k')$ involving $\Gamma(\hat{\Omega})$ and $\Gamma'(\hat{\Omega})$ can be described in terms of the all-sky cross-spectra $C_l^{\Gamma\Gamma'}(k, k')$ and a mode-mixing matrix G that describes the effect of mode-mode coupling resulting from the presence of the mask. The mode-mixing matrix depends on the spin-weight of the respective fields s and s' and also depends on the power spectrum of the mask w_l .

$$\tilde{C}_l^{\Gamma\Gamma'}(k, k') \equiv \frac{1}{2l+1} \sum_m [{}_s\tilde{\Gamma}]_{lm}(k) [{}_{s'}\tilde{\Gamma}']_{lm}(k') \equiv \frac{1}{2l+1} \sum_m [{}_s\Gamma w]_{lm}(k) [{}_{s'}\Gamma' w]_{lm}(k') \approx \sum_{l'} G_{ll'} C_{l'}^{\Gamma\Gamma'} \left[\frac{2l+1}{2l'+1} k, \frac{2l+1}{2l'+1} k' \right]; \quad (14)$$

$$G_{ll'} = \frac{1}{4\pi} \sum_{l_a} \frac{(2l'+1)^2}{(2l+1)} (2l_a+1) \begin{pmatrix} l & l_a & l' \\ s & 0 & -s \end{pmatrix} \begin{pmatrix} l & l_a & l' \\ s' & 0 & -s' \end{pmatrix} |w_{l_a}|^2. \quad (15)$$

The radial direction remains unaffected by the mask which introduces mode mixing only on the surface of the celestial sphere hence the matrix M is independent of radial wave number k . For a given pair of radial wavenumbers k, k' the all-sky cross-spectra $C_l^{\Gamma\Gamma'}(k, k')$ can in principle be recovered by inverting the above expression Eq.(15). In general there will be contribution from noise which can be from intrinsic ellipticity or flexion distribution of galaxies in case of shear or flexion. Such contributions need to be subtracted to make any estimation unbiased, and there may be standard issues with inversion which may require regularisation.

To recover the power spectrum of E and B modes of a spin ± 2 fields, commonly used in the context of analysis of CMB polarization analysis, e.g. as in Brown, Castro & Taylor (2005), we have to express angular harmonics of ${}_s\Gamma = {}_{+2}\Gamma$ and ${}_{s'}\Gamma' = {}_{-2}\Gamma$ in terms of their Electric (E) and magnetic (B) components ${}_2\Gamma_{lm} = E_{lm} + iB_{lm}$. Then using Eq.(15) we can relate the cut-sky power spectra $\tilde{C}_l^{EE} = \frac{1}{2l+1} \sum_m \tilde{E}_{lm} \tilde{E}_{lm}^*$ and $\tilde{C}_l^{BB} = \frac{1}{2l+1} \sum_m \tilde{B}_{lm} \tilde{B}_{lm}^*$ in terms of their all-sky counterparts C_l^{EE} and C_l^{BB} . However Eq.(15) generalizes such results to generic spin functions with arbitrary spin-weights. For generic spin weight functions the cut-sky and all-sky relations are:

$$\mathcal{C}_l^{EE} = G_{ll'}^{EE} \mathcal{C}_{l'}^{EE} + G_{ll'}^{EB} \mathcal{C}_{l'}^{BB}; \quad \mathcal{C}_l^{BB} = G_{ll'}^{BE} \mathcal{C}_{l'}^{EE} + G_{ll'}^{BB} \mathcal{C}_{l'}^{BB} \quad (16)$$

A sum over repeated indices are assumed in each of these equations. The matrices $G_{ll'}^{EE}$, $G_{ll'}^{BB}$ and $G_{ll'}^{EB}$ are defined through the following expressions:

$$\begin{aligned} G_{ll'}^{EE} = G_{ll'}^{BB} &\equiv \frac{1}{8\pi} \sum_{l_a} \frac{(2l'+1)^2}{(2l+1)} (2l_a+1)(1+(-1)^L) \begin{pmatrix} l & l_a & l' \\ s & 0 & -s \end{pmatrix}^2 \\ G_{ll'}^{EB} = G_{ll'}^{BE} &\equiv \frac{1}{8\pi} \sum_{l_a} \frac{(2l'+1)^2}{(2l+1)} (2l_a+1)((-1)^L - 1) \begin{pmatrix} l & l_a & l' \\ s & 0 & -s \end{pmatrix}^2; \end{aligned} \quad (17)$$

It is interesting to notice here that instead of $\mathcal{C}_l(k_1, k_2)$ if we study $\Sigma(k_1, k_2) = \sum_l (2l+1) \mathcal{C}_l(k_1, k_2)$ they will have exactly similar mixing properties as the ordinary 2D fields, modulo the remapping of the radial harmonics, as the usual 3D power spectrum C_l when a mask is applied, i.e. $\tilde{\Sigma}^{\kappa\kappa}(k_1, k_2) = \sum_{l'} M_{ll'} \Sigma(\frac{2l'+1}{2l'+1} k_1, \frac{2l'+1}{2l'+1} k_2)$; where $G_{ll'} = \frac{(2l'+1)}{(2l+1)} M_{ll'}$. This property will be valid not just as the level of power spectrum but also for skew- and kurt spectra as well as for multispectra of arbitrary order.

We have plotted the projected power spectrum for convergence $\mathcal{C}_l^{\kappa\kappa}$ in Fig. (1) as a function of l (left panel). Two different redshifts were considered $z_s = 0.5$ and $z_s = 1.0$. The Λ CDM background cosmology that we will be using throughout this paper is characterised by the following set of parameters: $\Omega_m = 0.3$, $\Omega_\Lambda = 0.7$, $\Gamma = 0.21$, $h = 0.7$ and $\sigma_8 = 0.90$. The power spectra associated with other spinorial fields (shear and flexions) are also plotted (right panel). The 3D power spectrum $C_l^{\kappa\kappa, \kappa}$ is plotted in Fig. 4 for the same background cosmology. We plot $C_l^{\kappa\kappa, \kappa}(k, k)$ for three different choice of k values as function of l (left panel) as well as $C_l^{\kappa\kappa, \kappa}(k, k)$ for three selection of l values as a function of the radial wave number k .

3.2 Bispectrum

The power spectrum carries the bulk of the information in any cosmological observations. However often a set of degenerate cosmological scenarios can lead to a very similar power spectrum. Analysing higher-order correlation functions can lift this degeneracy to some extent. The non-Gaussianity used can be either due to primordial or secondary effects, and in the case of weak lensing the main source of non-Gaussianity comes from gravitational instability. Note that a non-zero bispectrum signifies the lowest-order departure from gaussianity, and its detection is generally easier than higher-order multispectra.

To make contact with the observables we use the fact that the convergence can be related directly to the 3D density field. We will start by linking the 3D convergence bispectrum \mathcal{B} and the 3D density bispectrum expressed in harmonic coordinates. In the next section we will express the bispectrum in spherical coordinate in terms of the bispectrum in rectangular coordinates and use some well-motivated approximations to simplify the results.

Statistical isotropy requires that

$$\langle \kappa_{l_1 m_1}(k_1; r_1) \kappa_{l_2 m_2}(k_2; r_2) \kappa_{l_3 m_3}(k_3; r_3) \rangle = \begin{pmatrix} l_1 & l_2 & l_3 \\ m_1 & m_2 & m_3 \end{pmatrix} \mathcal{B}_{l_1 l_2 l_3}^{\kappa\kappa}(k_i; r_i) \quad (18)$$

and using Eq.(6) we can write

$$\begin{aligned} \mathcal{B}_{l_1 l_2 l_3}^{\kappa\kappa}(k_i; r_i) &= A^3 \mathcal{L}_1 \mathcal{L}_2 \mathcal{L}_3 \left(\frac{2k_1}{\pi c^2} \right) \left(\frac{2k_2}{\pi c^2} \right) \left(\frac{2k_3}{\pi c^2} \right) \int_0^\infty \frac{dk'_1}{k'_1} \int_0^\infty dr_1 r_1^2 j_{l_1}(k'_1 r_1) j_{l_1}(k_1 r_1) \int_0^{r_1} \frac{dr'_1}{a(r'_1)} F_K(r_1, r'_1) \times \\ &\int_0^\infty \frac{dk'_2}{k'_2} \int_0^\infty dr_2 r_2^2 j_{l_2}(k'_2 r_2) j_{l_2}(k_2 r_2) \int_0^{r_2} \frac{dr'_2}{a(r'_2)} F_K(r_2, r'_2) \int_0^\infty \frac{dk'_3}{k'_3} \int_0^\infty dr_3 r_3^2 j_{l_3}(k'_3 r_3) j_{l_3}(k_3 r_3) \int_0^{r_3} \frac{dr'_3}{a(r'_3)} F_K(r_3, r'_3) \mathcal{B}_{l_1 l_2 l_3}^\delta(k'_i; r'_i); \\ &\mathcal{L}_i = l_i(l_i + 1) \sim l_i^2. \end{aligned} \quad (19)$$

The bispectrum $\mathcal{B}_{l_1 l_2 l_3}^{\kappa\kappa}(k_i; r_i)$ can now expressed in terms of the underlying matter bispectrum B^δ . The above relation mixes modes only in the radial directions r , and on the surface of the sky there is no mixing of angular harmonics if there is no sky mask. While expressing the density harmonics in terms of the 3D potential harmonics, we pick up additional scale factor $a(r_i)$ and wavenumber k_i dependence in the denominator.

We have so far ignored the presence of noise. Indeed because of the limited number of galaxies available it may not be possible to probe individual modes of the bispectrum at high signal-to-noise ratio. In later sections we will be able to address issues related to optimum combinations of individual modes which may be better suited for observational studies.

The convergence bispectrum can be written in terms of the density bispectrum as follows, using the Limber approximation to simplify the results:

$$\begin{aligned} \mathcal{B}_{l_1 l_2 l_3}^{\kappa\kappa}(k_i; r_i) &= H_1 H_2 H_3 \int_0^\infty r_1^2 dr_1 j_{l_1}(k_1 r_1) \int_0^\infty r_2^2 dr_2 j_{l_2}(k_2 r_2) \int_0^\infty r_3^2 dr_3 j_{l_3}(k_3 r_3) \mathcal{I}_{l_1 l_2 l_3}^{(3)}(r_1, r_2, r_3); \quad H_i \equiv A \frac{k_i}{c^2} \sqrt{\frac{2}{\pi}} \\ \mathcal{I}_{l_1 l_2 l_3}^{(3)}(r_1, r_2, r_3) &\equiv S_{l_1 l_2 l_3} b_{l_1 l_2 l_3} = S_{l_1 l_2 l_3} \int_0^{r_{min}} r^2 dr B^\delta \left(\frac{l_1}{r}, \frac{l_2}{r}, \frac{l_3}{r}; r, r, r \right) \mathcal{R}_1(r) \mathcal{R}_2(r) \mathcal{R}_3(r); \quad \mathcal{R}_i(r) = \frac{F_K(r_i, r)}{a(r)}. \\ S_{l_1 l_2 l_3} &= \sqrt{\frac{(2l_1+1)(2l_2+1)(2l_3+1)}{4\pi}} \begin{pmatrix} l_1 & l_2 & l_3 \\ 0 & 0 & 0 \end{pmatrix}. \end{aligned} \quad (20)$$

To derive this result we have used the extended Limber approximation Eq.(A2) to simplify the k'_i integrals. The integral here extends to the overlapping region i.e. $r_{min} = \min(r_1, r_2, r_3)$. In particular we can use the gravity-induced bispectrum here, or include others, such as a primordial bispectrum.

It is possible to simplify further the above expression using Eq.(A1):

$$\mathcal{B}_{l_1 l_2 l_3}^{\kappa \kappa \kappa} [k_1, k_2, k_3] = [Ac^{-2}]^3 \left[\frac{1}{k_1 k_2 k_3} \right]^2 \left[\frac{2l_1 + 1}{2} \right]^{3/2} \left[\frac{2l_2 + 1}{2} \right]^{3/2} \left[\frac{2l_3 + 1}{2} \right]^{3/2} S_{l_1 l_2 l_3} \mathcal{I}_{l_1 l_2 l_3}^{(3)} \left(\frac{2l_1 + 1}{2k_1}, \frac{2l_2 + 1}{2k_2}, \frac{2l_3 + 1}{2k_3} \right). \quad (21)$$

We will use a generic hierarchical ansatz to model the matter correlation hierarchy. Such ansatz constructs multi-point correlation functions from the products of lower-order correlation functions. In the Fourier domain this will lead to the construction of multispectra from products of ordinary power spectra. Such models have been tested against simulations and are routinely used both for projected galaxy surveys and for 2D weak lensing surveys. At the level of bispectrum we have: $B(k_1, k_2, k_3, r) = Q_3[P(k_1, r)P(k_2, r) + P(k_2, r)P(k_3, r) + P(k_1, r)P(k_3, r)]$. More detailed modelling will make Q_3 a function of the wave vector triplet (k_1, k_2, k_3) e.g. in the halo model Cooray & Seth (2002) or in Hyper Extended Perturbation Theory (Scoccimarro et al 1998). While the expression derived above is for the convergence field κ , it can be used to construct the other bispectra involving shear or flexion:

$$\mathcal{B}_{l_1 l_2 l_3}^{\gamma \pm \kappa \kappa} (k_i) = F_{l_1}^{\gamma \pm} \mathcal{B}_{l_1 l_2 l_3}^{\kappa \kappa \kappa} (k_i); \quad \mathcal{B}_{l_1 l_2 l_3}^{\gamma \pm \gamma \pm \kappa} (k_i) = F_{l_1}^{\gamma \pm} F_{l_2}^{\gamma \pm} \mathcal{B}_{l_1 l_2 l_3}^{\kappa \kappa \kappa} (k_i); \quad \mathcal{B}_{l_1 l_2 l_3}^{\gamma \pm \gamma \pm \gamma \pm} (k_i) = F_{l_1}^{\gamma \pm} F_{l_2}^{\gamma \pm} F_{l_3}^{\gamma \pm} \mathcal{B}_{l_1 l_2 l_3}^{\kappa \kappa \kappa} (k_i); \quad (22)$$

Results involving flexion can be constructed replacing the form factor $F_l^{\gamma \pm}$ s with the ones for the flexions i.e. $F_l^{\mathcal{F}}$ or $F_l^{\mathcal{G}}$ defined accordingly. The radial dependence of convergence, shear or flexion harmonics are the same.

Mode coupling is introduced by the presence of an observational mask. It is not possible to deconvolve the effect of a mask while analyzing the bispectrum from a realistic survey, as the inversion is typically unstable. However later we will introduce a power spectrum associated with the bispectrum (the skew spectrum), which can be computed from realistic data in the presence of mask and deconvolution can be done in a way very similar to the estimation of power spectrum discussed previously.

If we assume the intrinsic shear and flexion of source galaxies to be distributed according to a Gaussian distribution, then they do not contribute to the estimated bispectrum, but this is, of course, an assumption. However even in this case the scatter or variance in estimation does get a contribution from such a source of noise.

It is important to realize the results derived above are generic. They do not depend on the specific model used as an example (hierarchical ansatz). If we replace the underlying bispectrum with a primordial bispectrum of a specific type (e.g. local) we can still use the formalism developed here to compute various relevant statistics, we will introduce later, e.g. the skew spectrum. Later we will also introduce an optimized estimator for the skew spectrum. This estimator is not only optimized to detect any specific type of non-Gaussianity but it can also give an estimate of leakage from a specific source of non-Gaussianity (e.g. gravity-induced) while estimating another (primordial).

3.3 Trispectrum

The trispectrum or, alternatively, the four-point correlation function can provide an important sanity check (Kamionkowski, Smith & Heavens 2010) to validate lower-order detection of non-Gaussianity based solely on the bispectrum. The trispectrum, being a four-point correlation function is generally harder to probe compared to the bispectrum. However, in cases where the bispectrum vanishes due to symmetry considerations, the trispectrum is the lowest probe to study gravity-induced non-Gaussianity. In addition, while the study of trispectrum is interesting in itself it is also important in the proper characterization of the error in the power spectrum. As in the case of bispectrum we will start by modelling the bispectrum of the convergence field which can then be generalised to model trispectra associated with various spinorial fields. These results will eventually be used to model two different power spectra associated with the trispectrum (the *kurt spectra*).

The convergence trispectrum $\mathcal{T}_{l_3 l_4}^{l_1 l_2} (L, k_i; r_i)$ is the four-point correlation function in the harmonic domain and can be expressed as

$$\langle \delta_{l_1 m_1} (k_1; r_1) \delta_{l_2 m_2} (k_2; r_2) \delta_{l_3 m_3} (k_3; r_3) \delta_{l_4 m_4} (k_4; r_4) \rangle_c = \sum_{LM} (-1)^M \begin{pmatrix} l_1 & l_2 & L \\ m_1 & m_2 & M \end{pmatrix} \begin{pmatrix} l_3 & l_4 & L \\ m_3 & m_4 & -M \end{pmatrix} \delta T_{l_3 l_4}^{l_1 l_2} (L, k_i; r_i). \quad (23)$$

The vectors l_1, l_2, l_3, l_4 represents the sides of a quadrilateral and L is the length of the diagonal. The matrices as before are the Wigner $3j$ symbols. The symbols are only non-zero when they satisfy several conditions; which are $|l_1 - l_2| \leq L \leq l_1 + l_2, |l_3 - l_4| \leq L \leq l_3 + l_4; l_1 + l_2 + L = \text{even}, l_3 + l_4 + L = \text{even}$ and $m_1 + m_2 = M$ as well as $m_3 + m_4 = -M$. In our notation for the trispectrum, $T_{l_3 l_4}^{l_1 l_2} (k_i, r_i; L)$, the indices $(k_i; r_i)$ encode their dependence on various Fourier modes of the density harmonics in the radial direction, used in their construction. No summation will assumed over these variables unless explicitly specified. To model the trispectrum we will relate it to the underlying trispectrum of the density distribution $T_{l_3 l_4}^{l_1 l_2} (k'_i; r'_i)$.

$$\begin{aligned} \kappa \mathcal{T}_{l_3 l_4}^{l_1 l_2} (k_i; r_i) &= A^4 \mathcal{L}_1 \mathcal{L}_2 \mathcal{L}_3 \mathcal{L}_4 \left(\frac{2k_1}{\pi c^2} \right) \cdots \left(\frac{2k_4}{\pi c^2} \right) \int_0^\infty \frac{dk'_1}{k'_1} \int_0^\infty dr_1 r_1^2 j_{l_1} (k'_1 r'_1) \int_0^{r_1} \frac{dr'_1}{a(r'_1)} F_K (r_1, r'_1) \\ &\quad \cdots \int_0^\infty \frac{dk'_4}{k'_4} \int_0^\infty dr_4 r_4^2 j_{l_4} (k'_4 r'_4) \int_0^{r_4} \frac{dr'_4}{a(r'_4)} F_K (r_4, r'_4) \delta T_{l_3 l_4}^{l_1 l_2} (k'_i; r'_i). \end{aligned} \quad (24)$$

The above expression is a direct consequence of Eq.(4). To make any further progress we need to consider a specific form for the matter trispectrum. There are two generic prescriptions for treating a gravity-induced trispectrum. The halo model is one, and has been developed over the last several years and is very popular for modelling the correlation hierarchy of the underlying mass-distribution. Another is that perturbative descriptions can also provide a reasonable description of the onset of non-linearity at comparatively larger length scales. The hierarchical ansatz on the other hand describes the matter correlation hierarchy in the highly non-linear regime on smaller length scales. It builds up the higher-order correlation hierarchy from the two-point correlation function. All possible *diagrams* that connect points at which the correlation function is being constructed are considered. These diagrams are attributed various amplitudes according to their topology. Different diagrams with same topologies are associated with same amplitude. At the level of the four-point correlation function there are only two different topologies *star* and *snake*. We will denote the corresponding amplitudes by R_b and R_a and consider each of these contributions separately next.

3.3.1 Star Diagrams

The star diagrams are easier to handle because topologically they consist of a single vertex and lack any internal momentum that needs to be integrated out. In generic hierarchical scenarios a *star* diagram appears at each order in the hierarchy. In the case of projected 2D analysis, it has been found that replacing all diagrams with the same number of star diagrams often is sufficient to reproduce all one-point statistical features of convergence maps (Munshi, Valageas & Barber 2004; Barber, Munshi & Valageas 2004; Valageas, Munshi & Barber 2005). However the results presented here are generic and includes both contributions.

The derivation of the star contribution to the convergence trispectrum follows a similar technique as the bispectrum. The first step is to express the density convergence in terms of the triplets of matter power spectra. Next, using the expression Eq.(4) we can relate the star contribution of convergence trispectra to that of underlying mass distribution:

$$\begin{aligned} \delta T_{l_3 l_4}^{l_1 l_2} \left(L, \frac{l_i}{r}; r_i \right)_{\text{star}} &= \left(\frac{2}{\pi} \right)^2 k_1 k_2 k_3 k_4 \int_0^\infty dr_1 r_1 j_{l_1}(k_1 r_1) \dots \int_0^\infty dr_4 r_4 j_{l_4}(k_4 r_4) J_{l_1 l_2 l_3 l_4}^{(4)}(r_1, r_2, r_3, r_4)_{\text{star}}, \quad \text{where} \\ J_{l_1 l_2 l_3 l_4}^{(4)}(k_i; r_i)_{\text{star}} &\equiv R_b S_{l_1 l_2 L} S_{l_3 l_4 L} \int r^2 dr j_{l_1}(k_1 r) \dots j_{l_4}(k_4 r) \{P(k_1; r_1) P(k_2; r_2) P(k_3; r_3) + \text{cyc.perm.}\}. \end{aligned} \quad (25)$$

The above equation is for the stellar contribution to the trispectrum of the underlying density distribution. The additional three terms can be recovered by cyclic permutation of the k_i variables. We can use this result next to express the convergence trispectrum. The simplification relies on the use of the extended Limber approximation to simplify the k_i integrals. Hierarchical ansatz and Limber approximations are both known to be valid at small scales which justifies their combined use (Munshi, Coles & Heavens 2010).

$$\begin{aligned} \kappa \mathcal{T}_{l_3 l_4}^{l_1 l_2} \left(L, \frac{l_i}{r}; r_i \right)_{\text{star}} &= H_1 H_2 H_3 H_4 \int_0^\infty r_1^2 dr_1 j_{l_1}(k_1 r_1) \dots \int_0^\infty r_4^2 dr_4 j_{l_4}(k_4 r_4) \mathcal{I}_{l_1 l_2 l_3 l_4}^{(4)}(r_1, r_2, r_3, r_4)_{\text{star}} \quad \text{where} \\ \mathcal{I}_{l_1 l_2 l_3 l_4}^{(4)}(r_1, r_2, r_3, r_4)_{\text{star}} &= R_b S_{l_1 l_2 L} S_{l_3 l_4 L} \int_0^{r^{\min}} r^2 dr \mathcal{R}_1(r) \dots \mathcal{R}_4(r) \left\{ P\left(\frac{l_1}{r}; r\right) P\left(\frac{l_2}{r}; r\right) P\left(\frac{l_3}{r}; r\right) + \text{cyc.perm.} \right\}. \end{aligned} \quad (26)$$

In generic hierarchical scenarios the trispectrum is a cubic combination of underlying matter power spectra, just as the convergence bispectrum is a quadratic function of matter power spectra. We will focus on a specific model, the hierarchical ansatz, to model the underlying density distribution. However as it was pointed out that similar techniques can also be applied in the context of more elaborate halo model prescription.

3.3.2 Snake Diagrams

The analysis of the snake diagrams is more difficult than that of the star diagrams. This is related to the fact that while higher-order *star* diagrams at each order are straightforward generalizations of the lower-order star diagrams, the *snake* diagrams are however constructed using two different lower-order star diagrams. The following expression was derived in Munshi, Coles & Heavens (2010) which relates the *star* contribution to convergence trispectra. In addition to various form factors, the following expression depends on the cubic product of the underlying matter power spectrum. The relative importance of star and snake differs in different models of the hierarchical ansatz, e.g. Szapudi & Szalay (1993, 1997) attributes equal weighting to both diagrams, whereas Bernardeau & Schaeffer (1992) constructs higher-order amplitudes from the lower-order star amplitudes. The amplitude of the new star diagram at each order is left arbitrary which can be fixed using simulations or through the use of hyper-extended-perturbation theory (Scoccimarro & Frieman 1999) which predicts one-point cumulants at each order. We note in passing that ordinary perturbation theory predicts a hierarchy similar to hierarchical ansatz at the onset of gravitational clustering. However the amplitudes in this regime for various topologies are different (Fry 1984).

$$\begin{aligned} \mathcal{Q}_{l_3 l_4}^{l_1 l_2} \left(L, \frac{l_i}{r}; r_i \right)_{\text{snake}}^{\text{sph}} &= H_1 H_2 H_3 H_4 \int_0^\infty r_1^2 dr_1 j_{l_1}(k_1 r_1) \dots \int_0^\infty r_4^2 dr_4 j_{l_4}(k_4 r_4) \mathcal{I}_{l_1 l_2 l_3 l_4}^{(4)}(r_1, r_2, r_3, r_4)_{\text{snake}} \\ \mathcal{I}_{l_1 l_2 l_3 l_4}^{(4)}(r_1, r_2, r_3, r_4)_{\text{snake}} &= R_a S_{l_1 l_2 L} S_{l_3 l_4 L} \int_0^{r^{\min}} r^2 dr \mathcal{R}_1(r) \dots \mathcal{R}_4(r) \left\{ P\left(\frac{l_1}{r}; r\right) P\left(\frac{l_3}{r}; r\right) P\left(\frac{l_2}{r}; r\right) + \text{cyc.perm.} \right\}. \end{aligned} \quad (27)$$

The cyc. perm. here represents a total of three other terms. These terms can be obtained by rearranging l_i s ($l_1 \rightarrow l_2$), ($l_3 \rightarrow l_4$) and ($l_1 \rightarrow l_2, l_3 \rightarrow l_4$). The other terms that can be obtained by considering two additional pairings by considering the exchanges ($l_2 \rightarrow l_3$) and ($l_2 \rightarrow l_4$). These will lead us to $\mathcal{Q}_{l_2 l_4}^{l_1 l_3}$ and $\mathcal{Q}_{l_3 l_2}^{l_1 l_4}$. The total number of *snake* terms considering three distinct pairings and permutations within each pairings is twelve. The snake contribution to trispectrum can be written as:

$$\begin{aligned} \mathcal{T}_{l_3 l_4}^{l_1 l_2} \left(L, \frac{l_i}{r}; r_i \right)_{\text{snake}}^{\text{sph}} &= \mathcal{Q}_{l_3 l_4}^{l_1 l_2} \left(L, \frac{l_i}{r}; r_i \right)_{\text{snake}}^{\text{sph}} + (2L+1) \sum_{L'} (-1)^{l_2+l_3} \left\{ \begin{matrix} l_1 & l_2 & L \\ l_4 & l_4 & L' \end{matrix} \right\} \mathcal{Q}_{l_2 l_4}^{l_1 l_3} \left(L', \frac{l_i}{r}; r_i \right)_{\text{snake}}^{\text{sph}} \\ &+ (2L+1) \sum_{L''} (-1)^{L+L''} \left\{ \begin{matrix} l_1 & l_2 & L \\ l_3 & l_4 & L'' \end{matrix} \right\} \mathcal{Q}_{l_3 l_2}^{l_1 l_4} \left(L'', \frac{l_i}{r}; r_i \right)_{\text{snake}}^{\text{sph}} \end{aligned} \quad (28)$$

The matrices in curly braces are the $6j$ symbols (Edmonds 1968). The differences in *snake* and *star* contributions are also apparent in various choices of permutations of ($l_1, l_2, l_3, l_4; L$) associated with individual terms.

The derivations outlined both for bispectrum and trispectrum are quite generic and depend only on the use of extended Limber approximation, and the analysis can be generalized to higher-order multispectra.

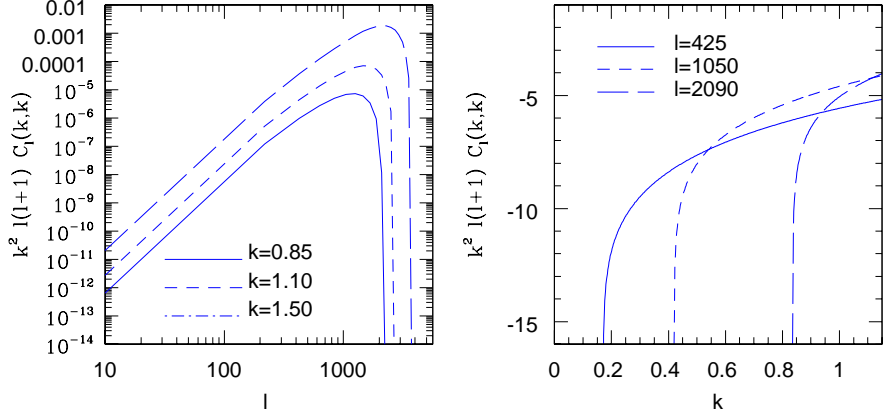


Figure 4. The left panel shows 3D power spectrum $l(l+1)k^2 C_l^{\kappa\kappa}(k, k)$ as a function of k for three different values of l . Where as the right panel shows $l(l+1)k^2 C_l^{\kappa\kappa}(k, k)$ as a function of k for fixed value of l . A LCDM background cosmology was assumed with $\Omega_m = 0.3, \Omega_\Lambda = 0.7, h = 0.7, \sigma_8 = 0.8, n_s = 1.0, w = -1$; we use an Eisenstein & Hu (1996) linear power spectrum and the Smith et al. (2003) non-linear correction. The sharp cutoff in these plots reflects survey depth through the Bessel inequality. Here k is displayed in hMpc^{-1} .

We will use these results to construct the power spectra associated with the trispectrum, or kurt spectra. Construction of trispectra for generic spin-weight functions can be achieved by using the form factors in a manner similar to the one adopted for the bispectrum Eq.(22).

$$\mathcal{T}_{\Gamma_{l_3}^{\prime\prime} \Gamma_{l_4}^{\prime\prime}}^{\Gamma_{l_1} \Gamma_{l_2}^{\prime}}(L, k_i) = F_{l_1}^{\Gamma} F_{l_2}^{\Gamma'} F_{l_3}^{\Gamma''} F_{l_4}^{\Gamma'''} \mathcal{T}_{l_3 l_4}^{l_1 l_2}(L, k_i) \quad (29)$$

The two different kurt spectra that we will construct next will provide independent probes of the underlying mass trispectra, and can play a valuable role in checking any cross-contamination from systematics.

4 POWER SPECTRA ASSOCIATED WITH MULTISPECTRA

The multispectrum may encode a great deal of information, but there is certain amount of degeneracy involved in it. Owing to the low signal-to-noise associated with the estimation of multispectra, it is impossible to estimate multispectra mode by mode. Estimation of multispectra is also hampered by their complicated response to the survey mask and complicated noise characteristics. Recent studies have shown that degenerate sets of power spectra can be constructed from multispectra at a given order. These compress some of the available information in the multispectra and can be computed from the observational data with relatively ease. We will construct the power spectra associated with bispectrum and trispectrum in this section. These power spectra were studied in some detail in (Munshi, Heavens & Coles 2010) in projection (2D). We generalize these results here to 3D. First we will obtain generic results, applicable irrespective of detailed analytical modelling of underlying multispectra. Next we will further specialize these results for the models outlined above, and we use extended Limber approximation to simplify the generic results.

4.1 skew spectrum

4.1.1 All-Sky Results

We will start by expanding the product of two generic spinorial fields with associated spin indices s, s' $[_s \Gamma_{s'} \Gamma'](\mathbf{r})$ in 3D in terms of their individual harmonics. The product of two spinorial fields with spins s and s' is a spinorial field of spin $s + s'$. The harmonic expansion therefore will have to be in terms of spin-weight spherical harmonics with spin index $s + s'$. In addition to expanding on the surface of the celestial sphere, we will also consider the expansion in the radial direction using spherical Bessel functions.

$$\begin{aligned} [_s \Gamma(\mathbf{r})_{s'} \Gamma'(\mathbf{r})]_{lm}(k) &= \sqrt{\frac{2}{\pi}} \int_0^\infty kr^2 dr j_l(rk) \int d\hat{\Omega} [_s \Gamma(\mathbf{r})_{s'} \Gamma'(\mathbf{r})]_{[s+s'] Y_{lm}^*(\hat{\Omega})} \\ &= \left(\frac{2}{\pi}\right)^{3/2} \int_0^\infty r^2 dr k j_l(rk) \sum_{l_i m_i} \int_0^\infty k_1 dk_1 j_l(k_1 r) [_s \Gamma_{l_1 m_1}(k_1)] \int_0^\infty k_2 dk_2 j_l(k_2 r) [_s' \Gamma'_{l_2 m_2}(k_2)] \int [{}_s Y_{l_1 m_1}(\hat{\Omega})] [{}_{s'} Y_{l_2 m_2}(\hat{\Omega})] [{}_{s+s'} Y_{lm}^*(\hat{\Omega})] d\hat{\Omega} \\ &= \left(\frac{2}{\pi}\right)^{3/2} \sum_{l_i m_i} \int_0^\infty dr kr^2 dr j_l(rk) \int_0^\infty k_1 dk_1 j_l(k_1 r) [_s \Gamma_{l_1 m_1}(k_1)] \int_0^\infty k_2 dk_2 j_l(k_2 r) [_s' \Gamma'_{l_2 m_2}(k_2)] \\ &\quad \times J_{l_1 l_2 l} \left(\begin{matrix} l_1 & l_2 & l \\ s & s' & -(s+s') \end{matrix} \right) \left(\begin{matrix} l_1 & l_2 & l \\ m_1 & m_2 & m \end{matrix} \right); \quad J_{l_1 l_2 l} = \sqrt{\frac{(2l_1+1)(2l_2+1)(2l+1)}{4\pi}}. \end{aligned} \quad (30)$$

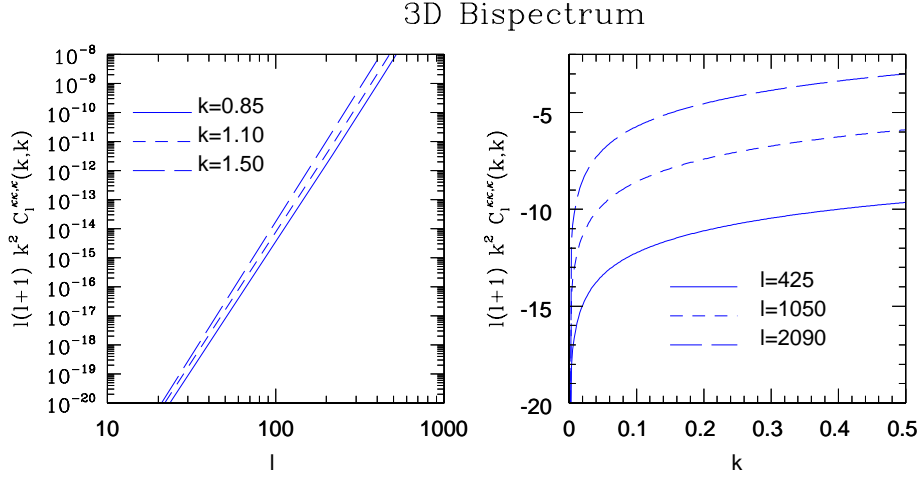


Figure 5. The right panel shows 3D power spectrum $l(l+1)k^2 C_l^{\kappa, \kappa}(k, k)$ as a function of k for three different values of l . Where as the left panel shows $l(l+1)k^2 C_l^{\kappa, \kappa}(k, k)$ as a function of l for fixed value of k . Three different k values were chosen as depicted. A Λ CDM background cosmology was assumed with $\Omega_m = 0.3$, $\Omega_\Lambda = 0.7$, $h = 0.7$, $\sigma_8 = 0.8$, $n_s = 1.0$; we use an Eisenstein & Hu (1996) linear power spectrum and the Smith et al. (2003) non-linear correction. A hierarchical ansatz was assumed for the bispectrum with the amplitude fixed at $Q = Q_3 = 1$. See text for more details. Here the wave vector k is displayed in units of hMpc^{-1} .

We have used the Gaunt integral to express integrals involving spherical harmonics in terms of the Wigner $3j$ symbols at the last step. The matrices describe the Wigner $3j$ symbols. To construct the skew spectrum, next we contract the multipole $[_s \Gamma(\mathbf{r})_{s'} \Gamma'(\mathbf{r}')]_{lm}$ with the multipole associated with a third spinorial 3D field $_{s''} \Gamma''_{lm}(k_3)$. The resulting skew spectrum or power spectrum associated with the bispectrum depends on the three radial wave numbers (k_1, k_2, k_3) , in addition to the spinorial indices associated with the respective 3D fields:

$$C_l^{\Gamma \Gamma', \Gamma''}(k, k') \equiv \frac{1}{2l+1} \sum_m [_s \Gamma_{s'} \Gamma']_{lm}(k) {}_{s''} \Gamma''_{lm}(k') \quad (31)$$

The bispectrum is defined by a triangular configuration in multipole space with lengths of side (l_1, l_2, l) . The power spectrum constructed above, will essentially capture information, through a summation, with all triangular configurations with one of these sides kept fixed at length l . If we now use the following expression for the 3D bispectrum $B_{l_1 l_2 l_3}^{\Gamma \Gamma', \Gamma''}(k_1, k_2, k_3)$ introduced earlier,

$$\mathcal{B}_{l_1 l_2 l_3}^{\Gamma \Gamma', \Gamma''}(k_1, k_2, k_3; r_i) = \sum_{m_1 m_2 m_3} \langle {}_s \Gamma_{l_1 m_1}(k_1; r_1) {}_{s'} \Gamma'_{l_2 m_2}(k_2; r_2) {}_{s''} \Gamma''_{l_3 m_3}(k_3; r_3) \rangle_c \begin{pmatrix} l_1 & l_2 & l_3 \\ m_1 & m_2 & m_3 \end{pmatrix}, \quad (32)$$

we can express the two-to-one power spectrum as:

$$C_l^{\Gamma \Gamma', \Gamma''}(k, k') = \left(\frac{2}{\pi} \right) \int_0^\infty r^2 dr k j_l(kr) \sum_{l_1 l_2} J_{l_1 l_2 l} \begin{pmatrix} l_1 & l_2 & l \\ s & s' & -(s+s') \end{pmatrix} \int_0^\infty k_1 dk_1 j_l(k_1 r) \int_0^\infty k_2 dk_2 j_l(k_2 r) \mathcal{B}_{l_1 l_2 l}^{\Gamma \Gamma', \Gamma''}(k_1, k_2, k'; r, r, r'). \quad (33)$$

Although the above relation is general and contains all the information regarding the evaluation of the skew spectrum for arbitrary spin-weight functions, the presence of multidimensional integrals makes it difficult to implement computationally.

We will simplify the results by using the extended Limber approximation to reduce the integrals involving k_1 and k_2 . First we express the \mathcal{B} in terms of the underlying matter bispectrum B using the expression Eq.(20). The extended Limber approximation, Eq. (A2), collapses the k_i integrals to one-dimensional Dirac delta functions. These delta functions are next used to reduce the r_1 and r_2 integrals. These simplifications which are known to be valid at high l . Finally we are left with two integrals involving r and r_3 which can be further simplified by Eq. (A3). The final expression contains only a one-dimensional integral and directly relates the skew spectrum $C_l^{\Gamma \Gamma', \Gamma''}(k, k')$ to the matter bispectrum:

$$C_l^{\Gamma \Gamma', \Gamma''}(k, k') = \sum_{l_1 l_2} \left[\frac{2}{2l_1+1} \frac{2}{2l_2+1} \frac{2}{2l+1} \right]^{\frac{1}{2}} J_{l_1 l_2 l} \left[\frac{2l_1+1}{2l+1} \right] k \left[\frac{2l_2+1}{2l+1} \right] k B_{l_1 l_2 l}^{\Gamma \Gamma', \Gamma''} \left[\frac{2l_1+1}{2l+1} k, \frac{2l_2+1}{2l+1} k, k' \right] \begin{pmatrix} l_1 & l_2 & l \\ s & s' & -(s+s') \end{pmatrix}. \quad (34)$$

Finally if we use the expression for the bispectrum derived using the same approximation, we can write:

$$C_l^{\Gamma \Gamma', \Gamma''}(k, k') = [Ac^{-2}]^3 \left[\frac{2}{2l+1} \right] \left[\frac{2l+1}{2k} \right]^2 \left[\frac{2l+1}{2k'} \right]^2 \sum_{l_1 l_2} J_{l_1 l_2 l}^2 \begin{pmatrix} l_1 & l_2 & l \\ 0 & 0 & 0 \end{pmatrix} \begin{pmatrix} l_1 & l_2 & l \\ s & s' & -(s+s') \end{pmatrix} I_{l_1 l_2 l}^{(3)} \left[\frac{2l+1}{2k}, \frac{2l+1}{2k}, \frac{2l+1}{2k'} \right] \\ I_{l_1 l_2 l_3}^{(3)}(r_1, r_2, r_3) = \int_0^\infty r^2 dr B^\delta \left[\frac{l_1}{r}, \frac{l_2}{r}, \frac{l}{r}; r, r, r \right] \mathcal{R}_1[r] \mathcal{R}_2[r] \mathcal{R}_3[r]; \quad \mathcal{R}_i[r] = \frac{F_{\mathbf{K}}(r_i, r)}{a(r)} \quad (35)$$

The bispectrum \mathcal{B} for convergence is defined in Eq.(19). The generic symbol $\mathcal{B}_{l_1 l_2 l}^{\Gamma \Gamma', \Gamma''}$ denotes the bispectrum for arbitrary spinorial fields as defined in

Eq.(32). Individual cases can be obtained by expressing $\mathcal{B}_{l_1 l_2 l}^{\Gamma, \Gamma'}$ in terms of the convergence bispectrum using the form factors introduced in Eq.(22). A numerical implementation of this result may not be easy due to associated computational cost.

The diagonal elements of the reduced bispectrum b_{lll} are plotted as a function of l in Fig. 2. We have plotted the projected skew spectrum for convergence $C_l^{\kappa, \kappa, \kappa}$ in Fig. 3. Two different redshifts were considered $z_s = 0.5$ and $z_s = 1.0$. The Λ CDM background cosmology that we have considered are described by the following set of parameters: $\Omega_M = 0.3$, $\Omega_\Lambda = 0.7$, $\Gamma = 0.21$, $h = 0.7$ and $\sigma_8 = 0.90$. We have taken a hierarchical form for the matter bispectrum and the amplitude Q_3 is set to unity. Changing the amplitude Q_3 only changes the overall normalization of the curve. Individual values of $C_l^{\Gamma, \Gamma'}$ at a given l depend on the modelling of the bispectrum for the entire range of l values being considered. Accurate modelling of the window function is therefore will be an important ingredient in such calculation. For our study we have considered a sharp cutoff in the multipole space at $l_{\max} = 2000$. The 3D skew spectrum $C_l^{\kappa, \kappa, \kappa}$ is plotted in Fig. 5 for the same background cosmology. We plot $C_l^{\kappa, \kappa, \kappa}(k, k)$ for three different choice of k values as function of l (left panel) as well as $C_l^{\kappa, \kappa, \kappa}(k, k)$ for three selection of l values as a function of the radial wave number k .

4.1.2 The Effect of a Sky Mask

A mask on the sky is defined through a generic function $w(\hat{\Omega}) = \sum_{lm} w_{lm} Y_{lm}(\hat{\Omega})$ on the surface of the sky. The mask can be a simple zero and one step function signifying masked and observed part of the sky or it can also be a more complex apodizing function with specific weights attach to the different parts of the sky. We will compute the skew spectrum in the presence of mask and express it in terms of the skew spectrum in the absence of any mask. This will allow us to eventually design an estimator which can estimate the unbiased skew spectrum from the real data in the presence of a mask and noise. We will consider Gaussian noise, which means that the estimation of bispectrum is not affected as the noise has vanishing skew spectrum; however the scatter associated with the estimator will change in the presence of noise. We will denote the masked power spectrum by \tilde{C}_l . We will see that convolved or masked skew spectrum is a linear sum of individual all-sky C_{ls} . This related to the fact that the use of mask introduces mode-mode correlation. A matrix inversion with suitable binning can produce the all-sky C_{ls} from the masked C_{ls} .

In our derivation we start by expanding the masked product field $[_s \Gamma(\mathbf{r})_{s'} \Gamma'(\mathbf{r}) w(\hat{\Omega})]$ in 3D and contract the resulting harmonics with the masked harmonics of another 3D spinorial field $[_{s''} \Gamma''(\hat{\Omega}) w(\hat{\Omega})]_{lm}^*$. The 3D harmonic expansion of the masked product field can be carried out using harmonics of spin index $s + s'$. Consequently the presence of a scalar spin-0 mask does not alter the spin of the product field which remains the same as the unmasked product field.

Repeated application of Gaunt's integral allows us to write the product harmonics in terms of the individual harmonics:

$$\begin{aligned}
 [_s \Gamma(\mathbf{r})_{s'} \Gamma'(\mathbf{r}) w(\hat{\Omega})]_{lm} &= \left(\frac{2}{\pi}\right)^{3/2} \sum_{l_i m_i} J_{l_1 l_2 l'} J_{l' l_a l} (-1)^{l+l'} \sum_{l_a m_a} w_{l_a m_a} s \Gamma_{l_1 m_1}(r) s' \Gamma'_{l_2 m_2}(r) \\
 &\quad \begin{pmatrix} l_1 & l_2 & l' \\ s & s' & -(s+s') \end{pmatrix} \begin{pmatrix} l_1 & l_2 & l' \\ m_1 & m_2 & -m' \end{pmatrix} \begin{pmatrix} l' & l_a & l \\ (s+s') & 0 & -(s+s') \end{pmatrix} \begin{pmatrix} l' & l_a & l \\ m' & m_a & -m \end{pmatrix}. \quad (36)
 \end{aligned}$$

The Fourier-Bessel decomposition of the quadratic field along the radial direction can be used to relate the 3D harmonics of the product field with that of individual constituent fields. This will eventually allow us to express the 3D skew spectrum in terms of the 3D bispectrum. The 3D skew spectrum presented here is a generalization of our previous work and incorporates full 3D information. This can be viewed also as a natural generalization of the 3D power spectrum presented in Castro et al (2005). Higher-order counterparts at the level of trispectrum will be presented in the next section.

$$\begin{aligned}
 [_s \Gamma(\mathbf{r})_{s'} \Gamma'(\mathbf{r}) w(\hat{\Omega})]_{lm}(k) &= \\
 &\left(\frac{2}{\pi}\right)^{3/2} \sum_{l_i m_i} J_{l_1 l_2 l'} J_{l' l_a l} (-1)^{l+l'} \int dr k r^2 j_l(kr) \sum_{l_a m_a} w_{l_a m_a} \int dk_1 j_{l_1}(rk_1) k_1 s \Gamma_{l_1 m_1}(r) \int dk_2 j_{l_2}(rk_2) k_2 s' \Gamma'_{l_2 m_2}(r) \\
 &\quad \times \begin{pmatrix} l_1 & l_2 & l' \\ s & s' & -(s+s') \end{pmatrix} \begin{pmatrix} l_1 & l_2 & l' \\ m_1 & m_2 & -m' \end{pmatrix} \begin{pmatrix} l' & l_a & l \\ (s+s') & 0 & -(s+s') \end{pmatrix} \begin{pmatrix} l' & l_a & l \\ m' & m_a & -m \end{pmatrix}. \quad (37)
 \end{aligned}$$

Construction of the masked skew spectrum follows the same approach. As we pointed out before the 3D skew spectrum has a radial wave number k dependence built in it. If we integrate the radial dependance out we can recover the usual projected skew spectrum. Expressing the skew spectrum in terms of the multipoles of squared field and individual fields (suitably masked),

$$\tilde{C}_l^{\Gamma, \Gamma'}(k, k') = \frac{1}{2l+1} \sum_{m=-l}^l [_s \Gamma(\hat{\Omega})_{s'} \Gamma'(\hat{\Omega}) w(\hat{\Omega})]_{lm}(k) [_{s''} \Gamma''(\hat{\Omega}) w(\hat{\Omega})]_{lm}^*(k, k'). \quad (38)$$

For the 3D harmonic decomposition $[_{s''} \Gamma''(\hat{\Omega}) w(\hat{\Omega})]_{lm}^*(k)$ of individual fields we use the expression derived previously in Eq.(13). Using these expressions for the multipoles in the presence of a mask from Eq.(37) and Eq.(13) and in Eq.(38) we can express the skew spectrum constructed from the masked multipoles or the pseudo skew spectrum in terms of a coupling matrix and the all-sky skew spectrum in 3D and a mode-coupling matrix. The mode-mode coupling matrix involves only the mask power spectra $w_l = \frac{1}{2l+1} \sum_m w_{lm} w_{lm}^*$, and depends on the spinorial indices of the respective 3D fields:

$$G_{ll'}^{ss's''} = \frac{1}{4\pi} \sum_{l_a} \frac{(2l'+1)^2}{(2l+1)} (2l_a+1) \begin{pmatrix} l & l_a & l' \\ s+s' & 0 & -(s+s') \end{pmatrix} \begin{pmatrix} l & l_a & l' \\ s'' & 0 & -s'' \end{pmatrix} |w_{l_a}|^2; \quad s, s', s'' \in 0, 1, \pm 2, 3; \quad (39)$$

The spin indices s, s', s'' take values 0 for κ , ± 2 for γ_{\pm} , -1 for F and 3 for G. After tedious but straightforward algebra along the line described in

Munshi, Heavens & Coles (2010) we can show that the pseudo- C_l s expressed as a linear combination of all-sky power spectra can now be expressed using the following relationship:

$$\tilde{C}_l^{\Gamma\Gamma',\Gamma''}(k, k') = \sum_{l'} G_{ll'}^{ss',s''} C_{l'}^{\Gamma\Gamma',\Gamma''} \left(\frac{2l+1}{2l'+1} k, \frac{2l+1}{2l'+1} k' \right). \quad (40)$$

The deconvolution process to recover the all-sky $C_{l'}^{\Gamma\Gamma',\Gamma''}(r_1, r_2)$ from its masked counterpart involves inversion of the coupling matrix G which depends not only l indices but also on spinorial indices associated with the fields. In case of small-sky coverage which might be the case for present generation of surveys, for inversion of the matrix will typically involve binning to avoid any possible numerically-singular matrices.

Here it is worth pointing out that the various spinorial fields that we can use to construct individual skew spectrum do probe the same underlying matter bispectrum. This can be used as a helpful diagnostic to probe possible spurious effects of mask and noise.

The power spectrum $C_l^{\Gamma\Gamma',\Gamma''}(k, k')$ reported here is an extension of similar power spectrum introduced in Munshi & Heavens (2009) for CMB studies. Later it was used in Munshi, Coles & Heavens (2010) to probe the convergence skew spectrum and was also generalized for projected spin-skew spectrum in (Munshi, Heavens & Coles 2010). In this study we present skew spectrum for spinorial fields using a complete 3D analysis. The power spectrum is specified by multipole indices on the surface of the celestial sphere as well as radial harmonics along the line of sight direction. Results are generic for fields with arbitrary spin and can be used to probe shear, flexion or convergence maps. Similar statistics in the coordinate space has been reported before. Bernardeau, van Waerbeke & Mellier (2003) studied $\langle \gamma^2(\hat{\Omega})\gamma(\hat{\Omega}') \rangle$ which directly deals with shear maps as opposed to convergence maps. This statistics along with a similar but simpler version which uses $\langle \kappa^2(\hat{\Omega})\kappa(\hat{\Omega}') \rangle$ was also studied. The perturbation theory was employed to model the underlying mass distribution and it used a flat sky approximation to simplify their calculations. A complementary statistic $\langle [\gamma(\hat{\Omega}_1) \cdot \gamma(\hat{\Omega}_2)]\gamma \rangle$ was also considered which relies on more detailed modelling of the bispectrum. These statistics were used by Bernardeau, Mellier & Van Waerbeke (2002) later to detect non-Gaussianity from the VIRMOS-DESCART Lensing Survey.

Our results presented here deal with power spectrum associated with the higher-order multispectra, are derived using generic all-sky treatment, and can also handle decomposition into Electric and Magnetic components in a much more straightforward manner. The results presented here are not only applicable to shear or convergence but are also applicable for higher-order spinorials such as *Flexions*. To increase the signal-to-noise of the estimates it is customary to often sum all possible mode of $C_l^{\Gamma\Gamma',\Gamma''}(k, k')$ in to a single number which is called *skewness*.

$$S_3^{\Gamma\Gamma',\Gamma''}(k, k') = \sum_l (2l+1) C_l^{\Gamma\Gamma',\Gamma''}(k, k') \quad (41)$$

For a concrete expression for $S_3^{\Gamma\Gamma',\Gamma''}(k, k')$ we need to replace $C_l^{\Gamma\Gamma',\Gamma''}(k, k')$ by the expression derived in Eq.(35) or Eq.(33).

To make connection with the real space statistics we can use the following relation:

$$C_l^{\Gamma\Gamma',\Gamma''}(k, k') = \frac{2}{\pi} \int dk k r^2 j_l(kr) \int dk' k' r'^2 j_l(k'r') \mathcal{D}_l^{\Gamma\Gamma',\Gamma''}(r, r'), \quad (42)$$

and a similar relation can be derived for the skewness $S_3^{\Gamma\Gamma',\Gamma''}(r, r')$ and $S_3^{\Gamma\Gamma',\Gamma''}(k, k')$ defined above. One point statistics such as $S_3(k, k')$ only contain radial information as all spherical harmonics are already summed over.

If we make the approximation of replacing the spherical Bessel function with a delta-function form we can write

$$C_l^{\Gamma\Gamma',\Gamma''}(k, k') = \frac{2}{2l+1} \mathcal{D}_l^{\Gamma\Gamma',\Gamma''} \left[\frac{2l+1}{2k}, \frac{2l+1}{2k'} \right]. \quad (43)$$

An equivalent expression is valid for $S_3^{\Gamma\Gamma',\Gamma''}(k, k')$. In both Eq.(42) and Eq.(43) we use the same notations to define the harmonic space $C_l^{\Gamma\Gamma',\Gamma''}(k, k')$ and real space $\mathcal{D}_l^{\Gamma\Gamma',\Gamma''}(r, r')$ power spectra. However their functional dependence on their arguments are different. It is interesting to notice that in Fourier domain the $C_l^{\Gamma\Gamma',\Gamma''}(k, k')$ probes specific length scales.

4.2 The Kurt spectrum

The four-point correlation function, or its harmonic counterpart the trispectrum, has been extensively studied in the literature . This contains the information about the non-Gaussianity beyond the lowest level (Hu 1999; Okamoto & Hu 2002).

For the case of weak lensing studies clearly the gravity-induced non-Gaussianity is the main motivation. Studies in trispectrum analysis have also been pursued using various other probes e.g. using 21-cm surveys (Cooray, Li & Melchiorri 2008) or more extensively in several CMB studies; see Bartolo et al (2004) for a review. However these studies typically probe the trispectrum induced by primordial non-Gaussianity. It is important to note that at the level of four-point, the Gaussian part of the signal as well as the noise both carry a non-zero (unconnected) trispectrum. This degrades the signal-to-noise for various estimators and clearly needs to be subtracted out before an unbiased comparison with the theoretical predictions can be made. It is obvious that the detection of the trispectrum from noisy data is far more nontrivial than the estimation of the bispectrum. We provide analytical expressions here mainly for completeness and to show that the generic results can be obtained based on very simple hierarchical ansatz.

Previous studies have mainly concentrated on one-point estimators which collapse the data to a single number - known as the kurtosis. We extend studies involving kurtosis $\langle [{}_s\Gamma_{s'}\Gamma'_{s''}\Gamma''_{s'''}\Gamma''''](\hat{\Omega}, r) \rangle$ to its two-point counterparts: $\langle [{}_s\Gamma_{s'}\Gamma'](\hat{\Omega}, r)[{}_{s''}\Gamma''_{s'''}\Gamma''''](\hat{\Omega}', r') \rangle$ and $\langle \Gamma\Gamma''(\hat{\Omega}, r)\Gamma''''(\hat{\Omega}', r') \rangle$. In practice however we will consider the Fourier transforms of these objects in 3D, the kurt spectra, which are the power spectra associated with the trispectra,

Table 1. Notations

Power Spectrum (R/F)	$\mathcal{D}_l(r_1, r_2), \mathcal{C}_l(k_1, k_2)$	Eq.(3.1)
Variance (R/F)	$\Sigma(r_1, r_2), \Sigma(k_1, k_2)$	Eq.(11)
Bispectrum	$B_{l_1 l_2 l_3}^\delta, B_{l_1 l_2 l_3}^{\kappa\kappa\kappa}, B_{l_1 l_2 l_3}^{\Gamma\Gamma\Gamma'}$	Eq.(18), Eq.(22)
Skew Spectrum (R/F)	$\mathcal{D}_l^{\Gamma\Gamma', \Gamma''}(r_1, r_2), \mathcal{C}_l^{\Gamma\Gamma', \Gamma''}(k_1, k_2)$	Eq.(33) Eq.(35)
Skewness (R/F)	$S_3^{\Gamma\Gamma', \Gamma''}(r_1, r_2), S_3^{\Gamma\Gamma', \Gamma''}(k_1, k_2)$	Eq.(41), Eq.(42)
Trispectrum	$\delta T_{l_3 l_4}^{l_1 l_2}, \kappa T_{l_3 l_4}^{l_1 l_2}$	Eq.(23)
Kurt Spectrum (R/F)	$\mathcal{D}_l^{\Gamma\Gamma', \Gamma''\Gamma'''}(r_1, r_2), \mathcal{C}_l^{\Gamma\Gamma', \Gamma''\Gamma'''}(k_1, k_2)$	Eq.(46)
	$\mathcal{D}_l^{\Gamma\Gamma', \Gamma''\Gamma'''}(r_1, r_2), \mathcal{C}_l^{\Gamma\Gamma', \Gamma''\Gamma'''}(k_1, k_2)$	Eq.(50)
Kurtosis(R/F)	$K_4^{\Gamma\Gamma', \Gamma''\Gamma'''}(r_1, r_2), K_4^{\Gamma\Gamma', \Gamma''\Gamma'''}(k_1, k_2)$	Eq.(51)
Deconvolution, Mixing Matrix	$\tilde{C}_l, \tilde{C}_l, M_{ll'}, G_{ll'}$	Eq.(15), Eq.(17), Eq.(39), Eq.(52)

$\mathcal{C}_l^{(\Gamma\Gamma', \Gamma''\Gamma''')}(k, k')$ and $\mathcal{C}_l^{(\Gamma\Gamma', \Gamma''\Gamma''')}(k, k')$. As was the case for the skew spectrum, we not only do harmonic decomposition on the surface of the celestial sphere but on as well on the radial direction. For the construction of $\mathcal{C}_l^{(\Gamma\Gamma', \Gamma''\Gamma''')}(k, k')$.

4.2.1 Two-to-Two Kurt Spectrum

The first of two kurt spectra $\mathcal{C}_l^{(\Gamma\Gamma', \Gamma''\Gamma''')}(k, k')$ can be constructed from the harmonic transform of $[\Gamma_{s'\Gamma'}]_{lm}(k)$ of the quadratic combination of two arbitrary spin-weight fields discussed previously in the context of the skew spectrum Eq.(30). The resulting kurt spectrum is generic and can be defined for any given set of four spin-weight functions defined in 3D. Unlike the skew spectrum which is zero for Gaussian fields, the kurt spectra are non-zero even in the absence of any non-Gaussianity, which introduces additional complexity. The Gaussian contribution (also known as the disconnected piece) needs to be subtracted out before it is employed for the study of non-Gaussianity. The noise, often assumed Gaussian, can also be subtracted following the same technique. It will contribute only to the disconnected part. Later in this section, we will also consider the effect of a mask as we did for the skew spectrum.

We will use these results to derive expressions for $\mathcal{C}_l^{(\Gamma\Gamma', \Gamma''\Gamma''')}(k, k')$ which leads to: $\mathcal{C}_l^{(\Gamma\Gamma', \Gamma''\Gamma''')}(k, k') = \frac{1}{2l+1} \sum_m [\Gamma_{s'\Gamma'}]_{lm}^*(k) [\Gamma_{s''\Gamma''}^*]_{lm}(k')$. These power spectra directly probe $T_{l_3 l_4}^{l_1 l_2}(l, k, k')$. It compresses all the available information in quadruplets of modes specified by (l_1, l_2, l_3, l_4) to a power spectrum. The power spectra $\mathcal{C}_l^{(\Gamma\Gamma', \Gamma''\Gamma''')}(k, k')$ and $\mathcal{C}_l^{(\Gamma\Gamma', \Gamma''\Gamma''')}(k, k')$ differ in the way they associate weights to various modes and contain complementary information. The reduced trispectrum $T_{l_1 l_2}^{l_3 l_4}(k_i; L)$ is defined in terms of $\langle s\Gamma_{l_1 m_1}(k_1) s'\Gamma'_{l_2 m_2}(k_2) s''\Gamma''_{l_3 m_3}(k_3) s'''\Gamma'''_{l_4 m_4}(k_4) \rangle_c$ as follows. We have added the radial distances r_i associated with each spherical harmonic in the argument with L , which specifies the diagonal formed by the quadruplet of four quantum numbers l_i $\langle s\Gamma_{l_1 m_1}(k_1) s'\Gamma'_{l_2 m_2}(k_2) s''\Gamma''_{l_3 m_3}(k_3) s'''\Gamma'''_{l_4 m_4}(k_4) \rangle_c = \sum_{LM} (-1)^M T_{l_3 l_4}^{l_1 l_2}(k_i; L) \begin{pmatrix} l_1 & l_2 & L \\ m_1 & m_2 & M \end{pmatrix} \begin{pmatrix} l_3 & l_4 & L \\ m_3 & m_4 & -M \end{pmatrix}$. The final expression depends on the spin indices of various fields as well as on a Kernel F (defined below) which has angular harmonic numbers l_i and radial wave numbers k, k' as its arguments:

$$\mathcal{C}_l^{(\Gamma\Gamma', \Gamma''\Gamma''')}(k, k') = \frac{1}{(2l+1)^2} \sum_{l_1 l_2 l_3 l_4} S_{l_1 l_2} S_{l_3 l_4} \begin{pmatrix} l_1 & l_2 & l \\ s_1 & s_2 & -(s_1 + s_2) \end{pmatrix} \begin{pmatrix} l_3 & l_4 & l \\ s_3 & s_4 & -(s_3 + s_4) \end{pmatrix} F^{(2,2)}(l_i, l, k, k'). \quad (44)$$

The kernel $F^{(2,2)}(l_i, l, k, k')$ is defined in terms of the reduced trispectrum $T_{l_3 l_4}^{l_1 l_2}(k_i; L)$.

$$F^{(2,2)}(l_i, l, k, k') = \left(\frac{2}{\pi}\right)^3 \int_0^\infty dr r^2 k j_l(kr) \int_0^\infty dr' r'^2 k' j_l(k'r') \\ \times \int_0^\infty dk_1 k_1 j_l(k_1 r) \int_0^\infty dk_2 k_2 j_l(k_2 r) \int_0^\infty dk_3 k_3 j_l(k_3 r') \int_0^\infty dk_4 k_4 j_l(k_4 r') T_{l_3 l_4}^{l_1 l_2}(k_i; L). \quad (45)$$

We will consider the two components of the trispectrum ‘‘snake’’ and ‘‘stars’’ separately for each of the two kurt spectra. If we follow the algebra, which is very similar to what was done previously to derive the skew spectrum we arrive at the following expression for the star component of the three-to-one kurt spectrum. The expression reduces to an one dimensional integral as we use the Limber approximation for simplification.

$$\mathcal{C}_l^{(\Gamma\Gamma', \Gamma''\Gamma''')}(k, k') = \frac{A^4}{c^8} \left[\frac{2}{2l+1} \right] \left[\frac{2l+1}{2k} \right]^2 \left[\frac{2l+1}{2k'} \right]^2 \frac{1}{(2l+1)^2} \\ \times \sum_{l_1 l_2 l_3 l_4} S_{l_1 l_2} S_{l_3 l_4} \begin{pmatrix} l_1 & l_2 & l \\ s_1 & s_2 & -(s_1 + s_2) \end{pmatrix} \begin{pmatrix} l_3 & l_4 & l \\ s_3 & s_4 & -(s_3 + s_4) \end{pmatrix} I_{tar}^{(4)} \left[\frac{2l+1}{2k}, \frac{2l+1}{2k}, \frac{2l+1}{2k'}, \frac{2l+1}{2k'} \right] \quad (46)$$

The contribution from the *star* diagram can be expressed in a similar manner. We simply have to replace the $I_{\text{snake}}^{(4)}$, which is defined in Eq.(27) with $I_{\text{star}}^{(4)}$ defined in Eq.(26). The additional terms that describe the exchange symmetry of snake terms however will involve the computation of $6j$ symbols Eq.(28) which poses additional computational complexity. There are two cumulant correlators at four-point level as explained above.

4.2.2 Three-to-One kurt spectrum

Following the discussion above we now focus on the other degenerate power spectra associated with the cumulant correlator $\langle [{}_s\Gamma_{s'}\Gamma''_{s''}\Gamma'''](\hat{\Omega})[{}_{s'''}\Gamma''''(\hat{\Omega}')] \rangle$. We will start by defining the all-sky harmonic transform $[\Gamma\Gamma'\Gamma'']_{lm}(k)$ for the cubic field ${}_s\Gamma_{s'}\Gamma''_{s''}\Gamma''(\hat{\Omega}, r)$ and cross-correlate it against the remaining field ${}_{s'''}\Gamma''''(k')$. This is of the same order as $\langle [{}_s\Gamma_{s'}\Gamma''(\hat{\Omega})[{}_{s'''}\Gamma''''(\hat{\Omega}')] \rangle$ and contains information about trispectra as well. The compression of the information is done with different weighting for different modes: $\mathcal{C}_l^{(\Gamma\Gamma'\Gamma'',\Gamma'''')}(k, k') = \frac{1}{2l+1} \sum_m \text{Real} \{ [{}_s\Gamma_{s'}\Gamma''_{s''}\Gamma''']_{lm}^*(k) [{}_{s'''}\Gamma''''_{lm}(k') \}$. We can now use the definition of the trispectra $T_{l_1 l_2}^{l_1 l_2}(L; k_1, k_2)$ to express $\mathcal{C}_l^{(\Gamma\Gamma'\Gamma'',\Gamma'''')}(k_1, k_2)$ in terms of the trispectra. The main difference with the previous spectrum $\mathcal{C}_l^{(\Gamma\Gamma',\Gamma''\Gamma'''')}(k_1, k_2)$ is that it sums over all possible configurations of the quadrilateral keeping one of the sides fixed, whereas $\mathcal{C}_l^{(\Gamma\Gamma',\Gamma''\Gamma'''')}(k_1, k_2)$ keeps one of the diagonals fixed but otherwise sums over all possible configuration of the quadrilateral. The harmonics of the cubic field can be expressed in terms of the individual harmonics using the following expressions. In the first equation we treat the radial direction using real-space expression and next we also do a Fourier transform in the radial direction to obtain a full 3D decomposition.

$$\begin{aligned} [{}_s\Gamma_{s'}\Gamma''_{s''}\Gamma''']_{lm}(r) &= \sum_{l_i m_i} {}_s\Gamma_{l_1 m_1}(r) {}_{s'}\Gamma'_{l_2 m_2}(r) {}_{s''}\Gamma''_{l_3 m_3}(r) \int d\hat{\Omega} Y_{l_1 m_1}(\hat{\Omega}) Y_{l_2 m_2}(\hat{\Omega}) Y_{l_3 m_3}(\hat{\Omega}) Y_{lm}^*(\hat{\Omega}) \\ [{}_s\Gamma_{s'}\Gamma''_{s''}\Gamma''']_{lm}(k) &= \left(\frac{2}{\pi}\right)^2 \int_0^\infty dr r^2 k j_l(kr) \sum_{l_i m_i} \int_0^\infty dk_1 k_1 j_{l_1}(k_1 r) \int_0^\infty dk_2 k_2 j_{l_2}(k_2 r) \int_0^\infty dk_3 k_3 j_{l_3}(k_3 r) {}_s\Gamma_{l_1 m_1}(k_1) {}_{s'}\Gamma'_{l_2 m_2}(k_2) {}_{s''}\Gamma''_{l_3 m_3}(k_3). \end{aligned} \quad (47)$$

Following these expression we can express the three-to-one kurt spectra in terms of the trispectrum. The geometric prefactors that appear in the projected (2D) three-to-one power spectra also appear in the 3D expression. The radial harmonics dependence comes through the kernel $F^{(3,1)}$:

$$\mathcal{C}_l^{(\Gamma\Gamma'\Gamma'',\Gamma'''')}(k_1, k_2) = \frac{1}{2l+1} \sum_{l_1 l_2 l_3; L} \frac{1}{2L+1} S_{l_1 l_2 L} S_{L l_3 l} \begin{pmatrix} l_1 & l_2 & L \\ s_1 & s_2 & -(s_1 + s_2) \end{pmatrix} \begin{pmatrix} L & l_3 & l \\ (s_1 + s_2) & s_3 & -(s_1 + s_2 + s_3) \end{pmatrix} F^{(3,1)}(l_i, l, k, k') \quad (48)$$

The kernel $F^{(3,1)}(l_i, l, k, k')$ is defined in terms of the trispectrum $T_{l_1 l_2}^{l_1 l_2}(k_i; L)$ as follows:

$$F^{(3,1)}(l_i, l, k, k') = \left(\frac{2}{\pi}\right)^3 \int_0^\infty dr r^2 k j_l(kr) \int_0^\infty dk_1 k_1 j_{l_1}(k_1 r) \int_0^\infty dk_2 k_2 j_{l_2}(k_2 r) \int_0^\infty dk_3 k_3 j_{l_3}(k_3 r) T_{l_3 l_4}^{l_1 l_2}(k_i; L). \quad (49)$$

The star contribution can be expressed in terms of the kernel $I_{\text{star}}^{(4)}$, using the Limber approximation:

$$\begin{aligned} \mathcal{C}_l^{(\Gamma\Gamma'\Gamma'',\Gamma'''')}(k, k') &= \frac{A^4}{c^8} \left[\frac{2}{2l+1} \right] \left[\frac{2l+1}{2k} \right]^2 \left[\frac{2l+1}{2k'} \right]^2 \frac{1}{(2l+1)^2} \\ &\times \sum_{l_1 l_2 l_3 l_4} S_{l_1 l_2} S_{l_3 l_4} \begin{pmatrix} l_1 & l_2 & L \\ s_1 & s_2 & -(s_1 + s_2) \end{pmatrix} \begin{pmatrix} L & l_3 & l \\ s_1 + s_2 & s_3 & -(s_1 + s_2 + s_3) \end{pmatrix} I_{\text{star}}^{(4)} \left[\frac{2l+1}{2k}, \frac{2l+1}{2k}, \frac{2l+1}{2k}, \frac{2l+1}{2k'} \right]. \end{aligned} \quad (50)$$

For the *snake* component, we need to replace the kernel $I_{\text{star}}^{(4)}$ with $I_{\text{snake}}^{(4)}$ which also involves a single integration. The evaluation of *snake* terms are however difficult as in addition there will be terms that involve $6j$ symbols Eq.(28) because of their permutation symmetry. As was the case with skew spectrum, we can collapse these fourth order two-point objects to reduce them to one-point numbers, the kurtosis, which will be a function of both radial harmonics k_1, k_2 :

$$K_4^{\Gamma\Gamma',\Gamma''\Gamma''''}(k_1, k_2) = \sum_l (2l+1) \mathcal{C}_l^{(\Gamma\Gamma',\Gamma''\Gamma'''')}(k_1, k_2); \quad K_4^{\Gamma\Gamma'\Gamma''\Gamma''''}(k_1, k_2) = \sum_l (2l+1) \mathcal{C}_l^{(\Gamma\Gamma'\Gamma''\Gamma'''')}(k_1, k_2). \quad (51)$$

The corresponding real space (in radial direction) versions $K_4^{\Gamma\Gamma',\Gamma''\Gamma''''}(r_1, r_2)$, and $K_4^{\Gamma\Gamma'\Gamma''\Gamma''''}(r_1, r_2)$ can be related using an equation similar to Eq.(42).

We will deal with the mode coupling issues arising from the partial sky coverage next. We will show how to deconvolve the effect of mask. It is important to keep in mind that the one point objects such as $K_4^{\Gamma\Gamma',\Gamma''\Gamma''''}(k_1, k_2)$ will have more signal-to-noise and can play important role in studying growth of non-Gaussianity along the radial direction.

A few general comments are in order. At the level of the trispectrum there are two hierarchical amplitudes. If we employ the two sets of kurt spectra then the amplitudes can be determined. This is very similar to their use in the CMB where the kurt spectra can be used to provide independent constraints for parameters g_{NL} and τ_{NL} that describe the Taylor expansion of the inflationary potential (Hu 1999; Okamoto & Hu 2002). Indeed in some hierarchical models the *snake* amplitude R_a and the bispectrum amplitude are related by $R_a = Q^2$. Similar relation also exists between f_{NL} and τ_{NL} . The study of skew spectrum can provide direct estimates of the parameter Q_3 . The estimates from skew spectrum is expected to be more significant statistically due to the higher signal-to-noise. An independent estimation using kurt spectra can provide a direct test of various hierarchical ansatz. It is important to realize that the skew

spectra as well as the kurt spectra are integrated quantities, i.e. their amplitudes at a specific l depends on the entire range of l values being considered. In terms of modelling of these quantities, it means that any successful theoretical prediction will have to correctly model the relevant multi-spectra for the entire range of l values being probed. The procedure can be extended to even higher-order. The number of distinct topological diagrams that are needed to build a correlation function at a given order will be same as the number of related power spectra, e.g. at fifth order there are three topological amplitudes and three multispectra. The procedure outlined above can be extended in such cases as signal to noise of the available data improves.

4.2.3 The effect of a Mask and Subtraction of Gaussian Contribution

The partial sky coverage will mean that the measured power spectrum $\tilde{\mathcal{C}}_l^{(\Gamma\Gamma'\Gamma''\Gamma''')}(k_1, k_2)$ is not the same as theoretical expectation, but is related as before by: $\tilde{\mathcal{C}}_l^{(\Gamma\Gamma'\Gamma''\Gamma''')}(k, k') = G_{ll'}\mathcal{C}_l^{(\Gamma\Gamma'\Gamma''\Gamma''')}(k, k')$. In fact it can shown that for arbitrary sky coverage with arbitrary mask the above analysis can be generalized to arbitrary order of correlation hierarchy. If we consider a correlation function at $p+q$ order, for every possible combination of (p, q) we will have an associated power spectrum. Using the same expression for the mode mixing matrix, we can invert the observed $\tilde{\mathcal{C}}_l^{(p,q)}(k_1, k_2)$ to $\hat{\mathcal{C}}_l^{(p,q)}(k_1, k_2)$. Hence for an arbitrary mask with arbitrary weighting functions the deconvolved set of estimators can be written as: $\hat{\mathcal{C}}_l^{(p,q)}(k_1, k_2) = \sum_{l'} G_{ll'}^{-1} \tilde{\mathcal{C}}_{l'}^{(p,q)}\left(\frac{2l'+1}{2l+1}k_1, \frac{2l'+1}{2l+1}k_2\right)$. The matrices G (defined below) depend on the spin indices as well as the power spectrum of the mask.

$$\begin{aligned} G_{ll'}^{ss's''s'''} &= \frac{1}{4\pi} \sum_{l_a} \frac{(2l'+1)^2}{2l+1} (2l_a+1) \begin{pmatrix} l & l_a & l' \\ s+s' & 0 & -(s+s') \end{pmatrix} \begin{pmatrix} l & l_a & l' \\ s''+s''' & 0 & -(s''+s''') \end{pmatrix} |w_{l_a}|^2; \\ G_{ll'}^{ss's''s'''} &= \frac{1}{4\pi} \sum_{l_a} \frac{(2l'+1)^2}{2l+1} (2l_a+1) \begin{pmatrix} l & l_a & l' \\ (s+s'+s'') & 0 & -(s+s'+s'') \end{pmatrix} \begin{pmatrix} l & l_a & l' \\ s''' & 0 & -s''' \end{pmatrix} |w_{l_a}|^2; \quad s, s', s'', s''' \in 0, 1, \pm 2, 3. \end{aligned} \quad (52)$$

However, as pointed out before, if we define kurt spectra $\hat{\mathcal{C}}_l^{(p,q)}(k_1, k_2) = (2l+1)\tilde{\mathcal{C}}_l^{(p,q)}(k_1, k_2)$ we can use the same mode coupling matrices that are used in projection for the purpose of deconvolution. However the 3D treatment introduces a remapping of the radial mode due to the presence of a mask $\tilde{\mathcal{C}}_l^{(p,q)}(k_1, k_2) = \sum_{l'} M_{ll'}\mathcal{C}_l^{(p,q)}\left(\frac{2l'+1}{2l+1}k_1, \frac{2l'+1}{2l+1}k_2\right)$.

The Gaussian contribution to the trispectrum \mathcal{G} can be written as:

$$\begin{aligned} \mathcal{G}_{l_3 l_4}^{l_1 l_2}(k_1, k_2, k_3, k_4; L) &= (-1)^{l_1+l_3} \sqrt{(2l_1+1)(2l_3+1)} \mathcal{C}_{l_1}^{\Gamma, \Gamma'}(k_1, k_2) \mathcal{C}_{l_3}^{\Gamma'', \Gamma'''}(k_3, k_4) \delta_{L0} \delta_{l_1 l_2} \delta_{l_3 l_4} \\ &+ (2L+1) (-1)^{l_2+l_3+L} \delta_{l_1 l_3} \delta_{l_2 l_4} \mathcal{C}_{l_1}^{\Gamma, \Gamma''}(k_1, k_3) \mathcal{C}_{l_2}^{\Gamma', \Gamma'''}(k_2, k_4) + (2L+1) \mathcal{C}_{l_1}^{\Gamma, \Gamma'''}(k_1, k_4) \mathcal{C}_{l_2}^{\Gamma', \Gamma''}(k_2, k_3) \delta_{l_1 l_4} \delta_{l_2 l_3}. \end{aligned} \quad (53)$$

The various power spectra $\mathcal{C}_{l_1}^{\Gamma, \Gamma''}(k_1, k_3)$ above include contributions from signal and noise. Next we can compute the Gaussian contributions to $\mathcal{C}_l^{(\Gamma\Gamma'\Gamma''\Gamma''')}$ and $\mathcal{C}_l^{(\Gamma\Gamma'\Gamma''\Gamma''')}$ following the same procedure as before just by replacing the trispectrum $T_{l_3 l_4}^{l_1 l_2}$ with its Gaussian counterpart $G_{l_3 l_4}^{l_1 l_2}(k_i; L)$. Indeed we will have to keep the ordering correct for various l_i and their r_i counterparts. It is also important to realize that in computing the Gaussian contribution we will have to take into account both the signal and the noise \mathcal{C}_l s (assumed to be Gaussian), i.e. $\mathcal{C}_l = \mathcal{C}_l^S + \mathcal{C}_l^N$. We will denote the Gaussian contributions to the (three-to-one) kurt-spectra by $\mathcal{G}_l^{(\Gamma\Gamma'\Gamma''\Gamma''')}(k_1, k_2)$ and (two-to-two) $\mathcal{G}_l^{(\Gamma\Gamma', \Gamma''\Gamma''')}(k_1, k_2)$ respectively:

$$\begin{aligned} \mathcal{G}_l^{(\Gamma\Gamma'\Gamma''\Gamma''')}(k_1, k_2) &= \frac{1}{2l+1} \sum_{l_1 l_2 l_3; L} \frac{1}{2L+1} S_{l_1 l_2 L} S_{L l_3 l} \mathcal{G}_{l_3 l}^{l_1 l_2}(L, k_1, k_2); \\ \mathcal{G}_l^{(\Gamma\Gamma', \Gamma''\Gamma''')}(k_1, k_2) &= \frac{1}{(2l+1)^2} \sum_{l_1 l_2 l_3 l_4} S_{l l_1 l_2} S_{l l_3 l_4} \mathcal{G}_{l_3 l_4}^{l_1 l_2}(l, k_1, k_2). \end{aligned} \quad (54)$$

For realistic surveys with a mask, the unconnected (Gaussian) contributions to the total kurt spectrum, listed above, can be deconvolved in a manner identical to what we have presented before for the connected part of the total trispectrum. The mode mixing matrix for the Gaussian contribution is identical to what we have introduced in Eq.(52). From the estimated $\tilde{\mathcal{D}}_l^{(\Gamma\Gamma'\Gamma''\Gamma''')}(r_1, r_2)$ and $\tilde{\mathcal{D}}_l^{(\Gamma\Gamma', \Gamma''\Gamma''')}(r_1, r_2)$ these contributions need to be subtracted out before comparing them against the theoretical expectations $\mathcal{C}_l^{(\Gamma\Gamma', \Gamma''\Gamma''')}(k, k') = \frac{2}{2l+1} \mathcal{D}_l^{(\Gamma\Gamma', \Gamma''\Gamma''')} \left[\frac{2l+1}{2k}, \frac{2l+1}{2k'} \right]$. An equivalent expression holds for the Gaussian contributions that needs to be subtracted: $\mathcal{G}_l^{\Gamma\Gamma', \Gamma''\Gamma'''}(k_1, k_2)$ and $\mathcal{G}_l^{\Gamma\Gamma', \Gamma''\Gamma'''}(k_1, k_2)$.

We have so far only considered the gravity-induced trispectrum in our discussion. However the kurt spectra for primordial non-Gaussianity can be derived in a very similar manner by replacing the gravity-induced trispectrum with a corresponding model for the primordial trispectrum. However it is expected that gravity-induced non-Gaussianity will dominate the primordial ones at least at lower redshift.

5 ERROR ANALYSIS

In the previous section, we have derived the expression for the 3D power spectrum associated with convergence field and indicated how a similar analysis can be performed for other spinorial fields. Estimation of these power spectra from noisy data will however will always have to deal with issues such as noise and partial sky coverage. An estimator which can deal with such observational constraints was developed for the case of power spectra in Eq.(15). It is however clear that the estimation of power spectra to be meaningful for any cosmological study we need an approximate handle on the error-bars and their covariance.

The error analysis for the PCL estimator that was introduced, can be done using the formalism used in Munshi et al. (2009) which is based on pseudo-CIs formalism developed by various authors in the context of CMB data analysis (Efstathiou 2004, 2006; Brown, Castro & Taylor 2005). The contributions to the error covariance will have three different components. On large angular scales or small l the error will be dominated mainly by cosmic variance where as the high l or smaller angular scale it will mainly be dominated by noise due to the intrinsic ellipticity of galaxies.

5.1 Power spectrum

$\mathcal{C}_l^{\Gamma, \Gamma'}(k, k')$ defines the cross-spectra between two spinorial fields ${}_s\Gamma(\hat{\Omega})$ and ${}_{s'}\Gamma'(\hat{\Omega})$. That is $\tilde{\mathcal{C}}_l^{\Gamma, \Gamma'}(k, k') = \frac{1}{2l+1} \sum_m \text{Re}[\tilde{\Gamma}^{lm*}(k) \tilde{\Gamma}'_{lm}(k')]$. It is possible to derive the covariance of estimates under certain simplifying assumptions. The general principles for deriving these results are outlined in Munshi et al. (2009) and will not be repeated here, and we quote the results for the ordinary power spectra here. For simplicity we will only consider $s = s'$. In later subsections we will also consider covariance matrices for the skew spectrum. The covariance matrix of the estimates is $\langle \delta\mathcal{C}_l^{\Gamma, \Gamma'}(k) \delta\mathcal{C}_{l'}^{\Gamma, \Gamma'}(k') \rangle$, where $\delta\mathcal{C}_l^{\Gamma, \Gamma'}(k)$ are the deviations from the ensemble average $\langle \mathcal{C}_l^{\Gamma, \Gamma'}(k) \rangle$:

$$\begin{aligned} \langle \delta\mathcal{C}_l^{\Gamma, \Gamma'}(k, k') \delta\mathcal{C}_{l'}^{\Gamma, \Gamma'}(k, k') \rangle &\approx \Sigma_{ll'}^{SS}(k, k') + \Sigma_{ll'}^{SN}(k, k') + \Sigma_{ll'}^{NN}(k, k') \\ \Sigma_{ll'}^{SS}(k, k') &= \frac{1}{4\pi} \left\{ \sqrt{\mathcal{C}_l^{\Gamma, \Gamma}(k, k) \mathcal{C}_{l'}^{\Gamma, \Gamma}(k, k)} \sqrt{\mathcal{C}_l^{\Gamma', \Gamma'}(k', k') \mathcal{C}_{l'}^{\Gamma', \Gamma'}(k', k')} + \mathcal{C}_l^{\Gamma, \Gamma'}(k, k') \mathcal{C}_{l'}^{\Gamma, \Gamma'}(k, k') \right\} \sum_{l_\alpha m_\alpha} \begin{pmatrix} l & l_\alpha & l' \\ s & 0 & -s' \end{pmatrix}^2 |w_{l_\alpha}|^2 \\ \Sigma_{ll'}^{NN}(k, k') &= \frac{1}{4\pi} \sum_{l_\alpha m_\alpha} \begin{pmatrix} l & l_\alpha & l' \\ s & 0 & -s' \end{pmatrix}^2 \left\{ |[\sigma^{\Gamma, \Gamma} w]_{l_\alpha m_\alpha}(k, k) [\sigma^{\Gamma', \Gamma'} w]_{l_\alpha m_\alpha}^*(k', k')| + |[\sigma^{\Gamma, \Gamma'} w^2]_{l_\alpha m_\alpha}(k, k')|^2 \right\} \\ \Sigma_{ll'}^{SN}(k, k') &= \frac{1}{4\pi} \sum_{l_\alpha m_\alpha} \begin{pmatrix} l & l_\alpha & l' \\ s & 0 & -s' \end{pmatrix}^2 \left\{ |[\sigma^{\Gamma', \Gamma'} w]_{l_\alpha m_\alpha}(k', k') [w]_{l_\alpha m_\alpha} \sqrt{\mathcal{C}_l^{\Gamma, \Gamma}(k, k) \mathcal{C}_{l'}^{\Gamma, \Gamma}(k, k)} + \text{symm. term.} \right. \\ &\quad \left. + 2 |[\sigma^{\Gamma, \Gamma'} w]_{l_\alpha m_\alpha}(k, k') [w]_{l_\alpha m_\alpha} \sqrt{\mathcal{C}_l^{\Gamma, \Gamma'}(k, k') \mathcal{C}_{l'}^{\Gamma, \Gamma'}(k, k')} \right\}. \end{aligned} \quad (55)$$

The symm. term. can be constructed by exchanging k and k' as well as Γ and Γ' . We have divided the total contribution into three different components. The term $\Sigma_{ll'}^{SS}(k, k')$ is the cosmic variance contribution and depends on the target spectra but is independent of noise. The term $\Sigma_{ll'}^{NN}(k, k')$ signifies the noise contribution and finally $\Sigma_{ll'}^{SN}(k, k')$ is a cross term which gets contributions from both signal and noise. We have assumed that the noise is statistically uncorrelated but it varies with pixel-position in the sky; i.e. $\langle \Gamma(\hat{\Omega}, r) \Gamma'(\hat{\Omega}', r') \rangle = \sigma^{\Gamma, \Gamma'}(\hat{\Omega}, r, r') \delta_{2D}(\hat{\Omega} - \hat{\Omega}')$.

A detailed modelling of source distribution is required for 3D error estimates. The observational mask $w(\Omega)$ that we use is completely generic however our results uses completeness and orthogonality of spherical harmonics on the cut-sky. This means results will be accurate only for near all-sky coverage. The various window functions that we have introduced are constructed from the 3D harmonic transforms such as $[\sigma^2 w^2]_{LM}(k)$ and $[\sigma w]_{LM}(k)$ of maps constructed from 3D noise maps and the mask (2D). These window functions are assumed to be much sharper than any variation in the power spectra. However such an assumption is unlikely to pose a problem as the weak lensing power spectrum lacks features unlike that of the CMB. The above expression is expected to be reasonably accurate at high l regime where the noise dominates. The 3D harmonics that we have used in our derivation based on the following definitions:

$$\begin{aligned} [\sigma^{\Gamma, \Gamma'}(\hat{\Omega}) w(\hat{\Omega})]_{lm}(k, k') &\equiv \int [\sigma^{\Gamma, \Gamma'}(\hat{\Omega}, k, k') w(\hat{\Omega})] Y_{lm}^*(\hat{\Omega}) d\hat{\Omega} \\ \sigma^{\Gamma, \Gamma'}(\hat{\Omega}, k, k') &= \frac{2}{\pi} \int k dk' j_l(kr) \int k' dk' j_l(k'r') \sigma^{\Gamma, \Gamma'}(\hat{\Omega}, r, r') = \frac{2}{2l+1} \sigma^{\Gamma, \Gamma'} \left[\hat{\Omega}, \frac{2l+1}{k}, \frac{2l+1}{k'} \right]. \end{aligned} \quad (56)$$

In the final step we have used the Limber approximation. Similar terms such as $[\sigma^{\Gamma, \Gamma'}(\hat{\Omega}) w(\hat{\Omega})]_{lm}(k, k')$ can be dealt with in a similar manner. In practice the evaluation of these terms will depend on the redshift distribution of galaxies.

The deconvolution of the error-covariance matrix can be performed using a similarity transformation. It involves the mode-coupling matrix introduced before:

$\langle \delta\hat{\mathcal{C}}_l^{\Gamma, \Gamma'}(k, k') \delta\hat{\mathcal{C}}_{l'}^{\Gamma, \Gamma'}(k, k') \rangle = M_{lL}^{-1} \langle \delta\tilde{\mathcal{C}}_L^{\Gamma, \Gamma'}(k, k') \delta\tilde{\mathcal{C}}_{L'}^{\Gamma, \Gamma'}(k, k') \rangle M_{l'L'}^{-1}$. A sum over repeated indices is assumed in this equation. The mode-coupling matrix introduced here depends on the spins of the relevant fields involved s and s' Eq.(15). We will next extend this result to the skew spectrum of arbitrary spinorial fields. For higher-order spectra the results are more involved but they can be computed using the same techniques considered here.

5.2 Skew spectrum

The expression for the skew spectrum, valid in the high- l regime using the Limber approximation, is derived in Eq.(35). The estimator for the skew spectrum quoted in Eq.(38) depends on cross-correlating an arbitrary product field $[_s\Gamma_{s'}\Gamma]_{lm}(k)$ against a third field ${}_{s''}\Gamma''_{lm}(k')$.

In this section we compute the error-covariance under certain simplifying assumptions. We will start from our definition of skew spectrum Eq.(38) and quote the result for the covariance, which can be derived using similar procedure adopted for the derivation of covariance of the ordinary power spectrum. The results correspond to three generic fields Γ , Γ' and Γ'' with arbitrary spin weight s , s' and $s'' = s + s'$ respectively:

$$\langle \delta\mathcal{C}_l^{\Gamma\Gamma'\Gamma''}(k, k') \delta\mathcal{C}_{l'}^{\Gamma\Gamma'\Gamma''}(k, k') \rangle \approx \Sigma_{ll'}^{SS}(k, k') + \Sigma_{ll'}^{SN}(k, k') + \Sigma_{ll'}^{NN}(k, k'). \quad (57)$$

The individual terms in terms of noise and signal power spectra are as follows:

$$\begin{aligned}
 \Sigma_{ii'}^{SS}(k, k') &= \frac{1}{4\pi} \left\{ \sqrt{C_l^{\Gamma\Gamma', \Gamma\Gamma'}(k, k) C_{l'}^{\Gamma\Gamma', \Gamma\Gamma'}(k', k')} \sqrt{C_l^{\Gamma'', \Gamma''}(k, k) C_{l'}^{\Gamma'', \Gamma''}(k', k')} + C_l^{\Gamma\Gamma', \Gamma''}(k, k) C_{l'}^{\Gamma\Gamma', \Gamma''}(k', k') \right\} \\
 &\quad \times \sum_{l_a m_a} \begin{pmatrix} l & l_a & l' \\ s + s' & 0 & -(s + s') \end{pmatrix} \begin{pmatrix} l & l_a & l' \\ s'' & 0 & -s'' \end{pmatrix} |w_{l_a}|^2 \\
 \Sigma_{ii'}^{NN}(k, k') &= \frac{1}{4\pi} \sum_{l_a m_a} \begin{pmatrix} l & l_a & l' \\ s + s' & 0 & -(s + s') \end{pmatrix} \begin{pmatrix} l & l_a & l' \\ s'' & 0 & -s'' \end{pmatrix} \left\{ |w^2 \sigma^{\Gamma\Gamma, \Gamma\Gamma'}|_{l_a m_a}(k) [w^2 \sigma^{\Gamma'', \Gamma''}]_{l_a m_a}^*(k') + [w^2 \sigma^{\Gamma\Gamma', \Gamma''}(k, k')]^2 \right\} \\
 \Sigma_{ii'}^{SN}(k, k') &= \frac{1}{4\pi} \sum_{l_a m_a} \begin{pmatrix} l & l_a & l' \\ s + s' & 0 & -(s + s') \end{pmatrix} \begin{pmatrix} l & l_a & l' \\ s'' & 0 & -s'' \end{pmatrix} \left\{ 2 |w^2 \sigma^{\Gamma\Gamma', \Gamma''}|_{l_a m_a}(k) |w^2|_{l_a m_a} \sqrt{C_l^{\Gamma\Gamma', \Gamma''}(k, k) C_{l'}^{\Gamma\Gamma', \Gamma''}(k, k')} \right. \\
 &\quad \left. + |w^2 \sigma^{\Gamma\Gamma', \Gamma\Gamma'}|_{l_a m_a}(k) |w^2|_{l_a m_a} \sqrt{C_l^{\Gamma'', \Gamma''}(k, k) C_{l'}^{\Gamma'', \Gamma''}(k, k')} + |w^2 \sigma^{\Gamma'', \Gamma''}|_{l_a m_a}(k) |w^2|_{l_a m_a} \sqrt{C_l^{\Gamma\Gamma', \Gamma\Gamma'}(k, k') C_{l'}^{\Gamma\Gamma', \Gamma\Gamma'}(k, k')} \right\} \quad (58)
 \end{aligned}$$

The error-covariance depends on noise maps for the product field as well as the individual field. The noise in our analysis is not assumed constant and can vary with position. The terms such as $|w^2 \sigma^{\Gamma\Gamma, \Gamma\Gamma'}|_{l_a m_a}(k)$ can also be defined using expression similar to Eq.(56). It underlines the difficulty associated with an accurate error estimation beyond the power spectrum.

These results are based on various assumptions valid at high $-l$ regime. However for future, near all-sky surveys for which the harmonic description is more appropriate these results can provide a good handle on estimation errors. Alternatively the error-covariance can be computed using Monte-carlo simulations. Simulating multiple copies of the observed sky, with all observational details, can be computationally expensive. Hence, often simplifying assumptions are employed to compute the covariance. The approach developed here can play a complementary role in cross-checking and validating such results. The lower-order covariance such as what we have considered above typically depends on higher-order power spectra. It is customary to quote error bars associated with estimated power spectra. However it is important to note that the error-bars for the higher-order spectra such as the skew spectra may not be fully informative, as the probability distribution of the skew spectrum for a given l can be skewed. In such cases, the error bars still can give an idea of statistical scatter around the estimate.

The results for deconvolved PCL estimates for the skew spectrum can be computed using a similarity transformation: $\langle \delta \hat{C}_l^{\Gamma\Gamma', \Gamma''}(k, k') \delta \hat{C}_{l'}^{\Gamma\Gamma', \Gamma''}(k, k') \rangle = \sum_{LL'} G_{LL}^{-1} \langle \delta C_L^{\Gamma\Gamma', \Gamma''}(k, k') \delta C_{L'}^{\Gamma\Gamma', \Gamma''}(k, k') \rangle G_{L'L}^{-1}$. The mode-coupling matrix G is independent of the radial wave vector k but depends on all three spin indices Eq.(39). Higher-order multi-spectra such as the skew spectrum are typically more correlated and binning may be needed for non-singular inversion.

It is also possible to compute the cross-covariance of these estimators for power spectrum and the skew spectrum which can be used jointly. These can result in tighter cosmological constraints. The results can be derived using the techniques presented above. The coupling matrices are different for different spinorial fields. They depend on the spin indices of the constituent spinorial fields. The spinorial fields considered above are however completely generic. If we assume that the magnetic or B-mode is absent then further simplification can be achieved.

5.3 Optimal Estimators

The estimators that we have constructed can be generalised if we optimally weight the harmonics with an inverse variance weight. The generalized two-to-one power spectrum $S_l^{\Gamma\Gamma', \Gamma''}$ in this case takes the following form:

$$\begin{aligned}
 \hat{S}_l^{\Gamma\Gamma', \Gamma''}(k, k') &\equiv \frac{1}{2l+1} \sum_{l' l''} \Lambda \hat{B}_{ll' l''}^{\Gamma\Gamma', \Gamma''}(k, k, k') B_{l' l''}^{\Gamma\Gamma', \Gamma''}(k, k, k'); \\
 \Lambda^{-1} &= \left([C_l^{\Gamma\Gamma}(k, k) C_{l'}^{\Gamma\Gamma'}(k, k) C_{l''}^{\Gamma''\Gamma''}(k', k')]^{-1} + \text{cyc.perm.} \right) \quad (59)
 \end{aligned}$$

This particular result is valid for all-sky coverage. The denominator Λ is the scatter in the estimator in the Gaussian limit. For partial sky coverage a more elaborate treatment in line with Munshi & Heavens (2009) is required. In the absence of spherical symmetry due to lack of all-sky coverage or asymmetric noise, we will have linear terms in the estimator. The estimator constructed in this way can achieve maximum possible signal-to-noise for a given data set. The one-point counterpart for this estimator, denoted as S can be recovered by summing over angular harmonics l , i.e. $S^{\Gamma\Gamma', \Gamma''}(k, k') = \sum_l (2l+1) S_l^{\Gamma\Gamma', \Gamma''}(k, k')$. An interesting point which we note here is that the hierarchical ansatz is *factorizable* which will allow easy construction of optimal weights. In general the expressions for gravity-induced the bi- or trispectra are not factorisable. At bispectrum level we can use the skew spectrum estimator to recover the tree amplitude Q_3 and similar estimators can be designed for the kurt spectra. The two different kurt spectra will allow independent estimation of topological amplitudes R_a and R_b . However it is expected that signal to noise at the level of trispectrum will be low. These optimal estimators can be optimized to detect either the gravity-induced non-Gaussianity or different models of primordial non-Gaussianity. They can also be used to forecast cross-contamination in a specific estimator from various sources of non-Gaussianity.

It is worth repeating here that the next generation of weak lensing surveys will have nearly all-sky coverage. This will probe a wide range of angular scales. The most commonly used technique for statistical characterization of such surveys is real space analysis using two- or three-point correlation functions. One of the advantages of using the higher-order correlation hierarchy is its ability to extract information from a complex survey geometry due to partial sky coverage. However, the real space analysis introduces highly correlated measurements for various angular scales. These correlations are more dominant at small angular scales where most of the observational information is contained. The alternative is to use the harmonic space representation of the correlation functions, e.g. the multi-spectra that are being studied here. Though mathematically equivalent the power spectra or their higher-order generalizations are much less used in the context of weak lensing. However the theoretical interpretation of multispectra is much simpler and different harmonics are much less

correlated. The main difficulty in harmonic analysis is related to the partial sky coverage. Typically the mask consists of bright stars and saturated spikes where no lensing measurements can be performed. The analytical results presented here provide a general analysis of the problem these pose. The results relate the convolved and deconvolved power spectra that can be constructed from the higher-order multispectra. The deconvolution process consists of simple matrix inversion and can be performed for arbitrary sky coverage. For the case of convergence the matrix representing mode-mode coupling in the presence of mask is independent of the order of the multi-spectra being probed. However that is not the case for the case of shear or flexions. The formalism developed here also allows for computation of scatter or variance associated with various estimators.

6 CONCLUSIONS

It is now well accepted that the next generation of weak lensing surveys will play an important part in further reducing the uncertainty in fundamental cosmological parameters, including those that describe the evolution of equation of state of dark energy Refregier et al. (2010). They will also be instrumental in testing various alternative gravity models (e.g. Heavens, Kitching & Verde (2007); Amendola, Kunz & Sapone (2008); Benyon, Bacon & Koyama (2009); Schrabback et al. (2009); Kilbinger et al. (2009)). The power of weak lensing surveys largely depends on the fact that they can exploit both the angular diameter distance and the growth of structure to constrain cosmological parameters. It is therefore very important to develop analytical techniques and statistical tools that can fully exploit the potential of future weak lensing surveys.

Typically without the redshift information the data from weak lensing surveys are analyzed in projection for the entire source distribution. However it was found that by binning sources in a few photometric redshift bins the constraints improve (Hu 1999). In recent years a full 3D formalism which exploits the photometric redshifts of individual sources were developed. Such an approach does not involve any binning; see Heavens (2003); Castro et al (2005); Heavens et al (2006). Further studies along these lines demonstrate that 3D lensing can provide more powerful and tighter constraints on the dark energy equation of state parameter, and on neutrino masses (de Bernardis et al. 2009; Jimenez et al. 2010 2010), as well as testing braneworld and other alternative gravity models. These constitute the main science drivers for the future weak lensing surveys. Initial studies in weak lensing focused on two-point correlation functions or the power spectrum mainly due to the low signal-to-noise available for higher-order studies from most first generation surveys. With the availability of modern surveys it is useful to include the non-Gaussianity information in the data analysis pipeline (Takada & Jain 2004; Semboloni et al 2009) that can help to lift some of the degeneracies in estimation of cosmological parameters involving power spectrum alone.

In their recent work Munshi, Coles & Heavens (2010) have explored the possibility of extending the higher-order statistics of convergence to 3D. The main motivation of this work is to generalize those results to spinorial objects and perform a full 3D analysis for the higher-order statistics. In this sense this is also an extension of results derived in Munshi, Heavens & Coles (2010) which analyzed higher-order statistics of spinorial fields but only in projection (2D). The results here are valid for all-sky surveys. It depends on full 3D spherical harmonic decomposition on the surface of the sky as well as along the radial directions. Such an approach in analyzing the data from future surveys which will cover a large fraction of the sky.

The higher-order statistics of convergence κ , shear γ_{\pm} or flexions \mathcal{F} and \mathcal{G} depend on accurate modelling of the underlying density contrast δ . Various models are used, such as the hierarchical ansatz which we use here, known to be valid in the highly nonlinear regime. However the techniques developed here are generic and can also be used in association with other models such as the halo model.

The higher-order multispectra contain invaluable information. Some of these information is however degenerate because of symmetries associated with higher-order correlation functions. It is difficult to estimate the higher-order multispectra mode by mode because of the associated scatter involved in such estimation especially from a noisy data set. In Munshi & Heavens (2009), various power spectra (skew spectrum, kurt spectra) were introduced, that are associated with a multispectra of a given order and can be estimated in the presence of mask and noise. These spectra carry some of the information contents of the multispectra from which they are constructed. In our present study we express the skew spectrum and two degenerate kurt spectra of generic spinorial fields in terms of the bi- and trispectrum. This extends earlier results for the convergence (spin-0) field. Extending the previously introduced 3D power spectrum $C_l(k_1, k_2)$ to higher-order, we introduce a series of power spectra related to multispectra at each order. We have introduced the 3D skew spectrum $C_l^{\Gamma\Gamma',\Gamma''}(k_1, k_2)$ associated with the bispectrum of arbitrary triplets of spinorial fields $\Gamma, \Gamma', \Gamma''$. Analogously, at the level of trispectrum we have introduced two 3D kurt spectra $C_l^{\Gamma\Gamma'\Gamma'',\Gamma'''}(k_1, k_2)$ and $C_l^{\Gamma\Gamma',\Gamma''\Gamma'''}(k_1, k_2)$ for arbitrary choice of spinorial fields. These extends the skew- and kurt spectra defined in Munshi, Coles & Heavens (2010) where harmonic decomposition was performed only on the surface of the celestial sphere and a real space analysis was performed on the radial direction leading to a mixed representation of skew spectrum $C_l^{(2,1)}(r_2, r_1)$ as well as their higher-order counterparts i.e. the two kurt spectra $C_l^{(2,2)}(r_2, r_1)$ and $C_l^{(3,1)}(r_2, r_1)$.

The generic expression for the skew- and kurt spectra involve spherical Bessel functions. We simplified these radial integrals by using the Limber approximation, whose accuracy scales as $\mathcal{O}(\frac{1}{l^2})$. We show that at each order the Limber approximation can reduce the dimensionality of the integrals to unity which dramatically reduces computational cost. Both the Limber approximation and the hierarchical ansatz are accurate at smaller scales and their joint use can help us to compute the skew- and kurt- spectra very efficiently with reasonable accuracy, but the method can accommodate different models for nonlinear clustering.

We also present analytical results for dealing with a mask, via a pseudo- C_l approach, encapsulated in a mode-mixing matrix. The estimation of unbiased skew- or kurt spectra are done by simple inversion of the mixing matrix M , which depends on the spins associated with the spinorial fields. Some regularisation will normally be required. The presence of an observational mask typically only induces mode-mixing on the celestial sphere and not on the radial direction. We have also showed how our formalism presented here can be used also for the computation of scatter under certain simplifying assumptions in the presence of an observational mask, and we have identified individual terms that correspond to contributions from noise, partial sky coverage (cosmic variance) and cross terms.

The results presented here will be relevant for the study of cosmic magnification studies in 3D as well as in many other contexts where integrated radial information is used. The estimators for skew or kurt spectra that we have described here can be improved by inverse variance weighting of 3D harmonics. Finally, to summarize:

- We have studied higher-order multispectra in the context of 3D weak lensing surveys.
- We use a full 3D Fourier decomposition which employ spin-weight spherical harmonics.

- Our generic results are valid for arbitrary 3D spinorial objects.
- The results are relevant for convergence κ , magnification μ , shear γ_{\pm} as well as flexions \mathcal{F} and \mathcal{G} or an arbitrary scalar tracer field Φ .
- In our analysis we define power spectra $C_l(k_1, k_2)$ that are related to the bispectrum (skew spectra) and to the trispectrum (kurt spectra).
- We provide both all-sky exact results and corresponding approximate results using the Limber approximation.
- Use of Limber's approximation reduces multidimensional integrations along the radial direction to one-dimensional integrals.
- We show how the multi-spectra can be recovered from a masked sky in the presence of noise, and show how the presence of masks mixes modes not only on the surface of the sky but in the radial direction.
 - The modelling was done using the hierarchical ansatz but the formalism can work with any input underlying density multispectra.
 - Under certain simplifying approximations, we also obtain expressions for the covariance of our power spectra and skew spectra estimators.
 - We outline how inverse variance weights can be introduced and optimal estimators can be defined for the detection of a specific type of non-Gaussianity.
 - The formalism can be relevant in many other contexts where line-of-sight integrations of non-Gaussianities are performed or in studies involving cross-spectra or mixed-bispectra.

In this paper we have ignored many observational complexities for simplicity, such as that in a realistic survey the lensing potential can only be sampled at the discrete positions of galaxies, and the average number of source galaxies will decline with redshift. We also ignore photometric redshift errors.

7 ACKNOWLEDGEMENTS

DM and PC acknowledge support from STFC standard grant ST/G002231/1 at the School of Physics and Astronomy at Cardiff University, where this work was completed. It is a pleasure for DM to acknowledge useful discussions with Ludovic van Waerbeke and Joseph Smidt. TK is supported by STFC rolling grant number RA0888.

REFERENCES

- Amendola, L., Kunz M., Sapone D., 2008, JCAP, 04, 13
- Bacon D.J., Goldberg D.M., Rowe B.T.P., Taylor A.N., 2006, MNRAS, 365, 414
- Bacon D.J., Goldberg D.M., Astrophys.J. 619 (2005) 741
- Bacon D.J., Refregier A., Ellis R.S., 2000, MNRAS, 318,625
- Barber A.J., Munshi D., Valageas P., 2004, MNRAS, 347, 667
- Bartolo N., Komatsu E., Matarrese S., Riotto A., 2004, Phys.Rept., 402, 103
- Benyon E., Bacon D.J., Koyama K., 2009, astro-ph/0910.1480
- Bernardeau F., Schaeffer R., 1992, A&A, 255, 1
- Bernardeau F., Valageas P., 2000, A&A, 364, 1
- Bernardeau F., Van Waerbeke L., Mellier Y., 1997, A&A, 322, 1
- Bernardeau F., Mellier Y., Van Waerbeke L., 2002, A&A, 389, L28
- Bernardeau F., Mellier Y. van Waerbeke L., 2003, A&A, 389, L28
- Bernardeau F., van Waerbeke L., Mellier Y., 2003, A&A, 397, 405
- Bernardeau F., Colombi S., Gaztanaga E., Scoccimarro R., 2002, Phys.Rept.,367, 1
- Bernstein G.M. Jarvis M. 2002, AJ, 123, 583
- Bouchet F.R., Juszkiewicz R., Colombi S. Pellat R., 1992, ApJ, 394, L5
- Brown M.L., Castro P.G. & Taylor A.N., 2005,MNRAS, 360 1262
- Bunn et al. 2003, PRD 67, 023501,
- Castro P.G., Heavens A.F., Kitching T.D., 2005, Phys.Rev. D72, 023516
- Coles P., Melott A.L., Munshi D., 1999, ApJ, 521, L5
- Cooray A., 2001, Phys.Rev. D, 64, 043516
- Cooray A., 2001, astro-ph/0105440
- Cooray A., Seth R., 2002, Phys. Rep. 372, 1
- Cooray A., Hu W., ApJ,2002, 574, 2002
- Cooray A., 2006, PRL, 97, 261301
- Cooray A., Li C., Melchiorri A., 2008, Phys.Rev.D, 77,103506
- Creminelli P., Nicolis A., Senatore L., Tegmark M., Zaldarriaga M., 2006, JCAP, 5, 4
- de Bernardis F., Kitching T. D., Heavens, A., Melchiorri, A., 2009, Phys. Rev. D80, 123509
- Edmonds, A.R., Angular Momentum in Quantum Mechanics, 2nd ed. rev. printing. Princeton, NJ:Princeton University Press, 1968.
- Efstathiou G., 2004, MNRAS, 349, 603
- Efstathiou G., 2006, MNRAS, 370, 343
- Goldberg D.M. & Natarajan P. 2002, ApJ, 564, 65
- Goldberg D.M. & Bacon D.J. 2005, ApJ, 619, 741
- Fry J.N., 1984, ApJ, 279, 499
- Heavens A.F., 1998, MNRAS, 299, 805
- Heavens A.F., 2003, MNRAS, 343, 1327
- Heavens A. F., Refregier A., Heymans C.E., 2000, MNRAS, 319, 649

- Heavens A. F., Kitching T. D., Taylor A.N., 2006, MNRAS, 373, 105
- Heavens A. F., Kitching T. D., Verde L., 2007, MNRAS, 380, 1029
- Hivon E., Górski K. M., Netterfield C. B., Crill B. P., Prunet S., Hansen F., 2002, ApJ, 567, 2
- Hoekstra H., Yee H. K. C., Gladders M. D., 2002, ApJ, 577, 595
- Hu W., ApJ., 1999, 522, L21
- Hui L., ApJ.,1999, 519, L9
- Jain B, Seljak U., White S. Astrophys.J., 2000, 530, 547
- Jain B., Seljak U., 1997, ApJ, 484, 560
- Jarvis M., Bernstein G. & Jain B., 2004, MNRAS, 352, 338
- Jimenez R., Kitching T.D., Pena-Garay C., Verde L., 2010, arXiv:1003.5918
- Kaiser N. 1992. ApJ, 388, 272
- Kaiser N., Wilson G., Luppino G.A., astro-ph/0003338
- Kamionkowski M., Smith T., Heavens A.F., 2010, arXiv:1010.0251
- Kilbinger M., et al., 2009, A& A, 497, 677
- Kitching T.D., Heavens A. F., Verde L., Serra P., Melchiorri A., Phys.Rev. 2008, D77, 103008
- Limber D.N., 1954, ApJ, 119, 665
- LoVerde M., Afshordi N. 2008, Phys.Rev.D78, 123506
- Massey R. et al, 2007, Nature, 445, 286
- Massey et al, 2007, ApJS, 172, 239
- Munshi D., 2000, MNRAS, 318, 145
- Munshi D., Bernardeau F., Melott A.L., Schaeffer R.,1999, MNRAS, 303, 433
- Munshi D., Coles P., 2000, MNRAS, 313, 148
- Munshi D., Coles P., 2002, MNRAS.329, 797
- Munshi D., Coles P., 2003, MNRAS, 338, 846
- Munshi D. Heavens A., Coles P. 2010, arXiv:1002.2089
- Munshi D., Coles P., Melott A.L., 1999a, MNRAS, 307, 387
- Munshi D., Coles P., Melott A.L., 1999b, MNRAS, 310, 892
- Munshi D., Heavens A., 2010, MNRAS, 401, 2406
- Munshi D. et al. 2009 arXiv:0910.3693
- Munshi D., Jain B., 2000, MNRAS, 318, 109
- Munshi D., Jain B., 2001, MNRAS, 322, 107
- Munshi D., Melott A.L., Coles P., 1999, MNRAS, 311, 149
- Munshi D., Valageas P., 2005, RSPTA, 363, 2675
- Munshi D., Valageas P., Barber A. J., 2004, MNRAS, 350, 77
- Munshi D., Valageas P., van Waerbeke L., Heavens A., 2008, PhR, 462, 67
- Munshi D., Valageas P., Cooray A., Heavens A, 2009, arXiv:0907.3229, MNRAS, in press
- Munshi D., Smidt J., Heavens A., Coles P., Cooray A. arXiv:1003.5003, MNRAS, in press
- Munshi D., Heavens A., Coles P. arXiv:1003.5003, MNRAS, in press
- Mo H.J., Jing Y.P., White S.D.M. 1997, MNRAS, 284, 189
- Navarro J., Frenk C., White S.D.M 1996, ApJ, 462, 563
- Okamoto T, Hu W., Phys.Rev. 2002, D66, 063008
- Pen et al. 2003, ApJ, 592, 664
- Penrose R. & Rindler W. Spinors and Space-time (Cambridge UP, 1984 and 1986) Vol. I and II
- Press & Sechter 1974, Astrophys.J, 187, 425
- Refregier A. 2003, MNRAS, 338, 35
- Refregier A. & Bacon D. 2003, MNRAS, 338, 48
- Refregier et al., 2010, astro-ph/1001.0061
- Sachs R.K. & Wolfe A.M., 1967 ApJ,147, 73
- Schaeffer R., 1984, A&A, 134, L15
- Schrabback et al. 2009, astro.co 0911.0053
- Schneider P., Van Waerbeke L., Jain B., Kruse G., 1998, MNRAS, 296, 873, 873
- Schneider P., Er X., 2008, A&A, 485, 363
- Scoccimarro R. et al,Astrophys.J. 1998, 496 586
- Scoccimarro R., Frieman J.A. 1999, Astrophys.J. 520 35
- Seljak U., 2000, MNRAS, 318, 203
- Semboloni et al, 2008, MNRAS, 388, 991
- Semboloni E., Tereno I., van Waerbeke L, Heymans C., 2009, MNRAS, 397, 608
- Smith K. M., Zaldarriaga M., 2006, arXiv:astro-ph/0612571
- Stebbins A., arXiv:astro-ph/9609149
- Szapudi I., Szalay A.S., 1993, ApJ, 408, 43
- Szapudi I., Szalay A.S., 1997, ApJ, 481, L1
- Takada M., Jain B., MNRAS, 348 (2004) 897

- Takada M., Jain B., 2003, MNRAS, 344, 857
 Takada M., White M., 2001, ApJ, 601, L1
 Takada M. Jain B., 2009, MNRAS, 395, 2065
 Valageas P., 2009, A&A, 356, 771
 Valageas P., Munshi D., Barber A. J., 2005, MNRAS, 356, 386
 Valageas P., Munshi D., 2004, MNRAS, 354, 1146
 Valageas P., Barber A. J., Munshi D., 2004, MNRAS, 347, 654
 Varshalovich D.A. Moskalev A.N. Khersonskii, Quantum Theory of Angular Momentum World Scientific, 1988
 Vishniac E.T., 1987, 322, 597
 van Waerbeke L. et al. 2000, A&A, 358, 30
 van Waerbeke L. et al. 2002, A&A, 393, 369
 Wittman D. et al. 2000, Nature, 405, 143

APPENDIX A: USEFUL MATHEMATICAL RELATIONS

A1 Spherical Bessel Functions

The orthogonality relationship for the spherical Bessel functions is given by the following expression:

$$\int k^2 j_l(kr_1) j_l(kr_2) dk = \left[\frac{\pi}{2r_1^2} \right] \delta_{1D}(r_1 - r_2). \quad (\text{A1})$$

The extended Limber approximation is also implemented through the following approximate relation LoVerde & Afshordi (2008):

$$\int k^2 F(k) j_l(kr_1) j_l(kr_2) dk \sim \left[\frac{\pi}{2r_1^2} \right] F\left(\frac{l}{r_1}\right) \delta_{1D}(r_1 - r_2). \quad (\text{A2})$$

Thus, for high l , the spherical Bessel functions can be replaced by a Dirac delta function δ_{1D} :

$$\lim_{x \rightarrow \infty} j_l(x) = \sqrt{\frac{\pi}{2l+1}} \delta_{1D}\left(l + \frac{1}{2} - x\right). \quad (\text{A3})$$

A2 3j Symbols

The following properties of 3j symbols were used to simplify various expressions.

$$\sum_{l_3 m_3} (2l_3 + 1) \begin{pmatrix} l_1 & l_2 & l_3 \\ m_1 & m_2 & m_3 \end{pmatrix} \begin{pmatrix} l_1 & l_2 & l_3 \\ m'_1 & m'_2 & m_3 \end{pmatrix} = \delta_{m_1 m'_1}^K \delta_{m_2 m'_2}^K \quad (\text{A4})$$

$$\sum_{m_1 m_2} \begin{pmatrix} l_1 & l_2 & l_3 \\ m_1 & m_2 & m_3 \end{pmatrix} \begin{pmatrix} l_1 & l_2 & l'_3 \\ m_1 & m_2 & m'_3 \end{pmatrix} = \frac{\delta_{l_3 l'_3}^K \delta_{m_3 m'_3}^K}{2l_3 + 1} \quad (\text{A5})$$

